catalysts

MDPI

Review

Which Configuration of Photocatalytic Membrane Reactors Has a Major Potential to Be Used at an Industrial Level in Tertiary Sewage Wastewater Treatment?

Raffaele Molinari *, Angela Severino, Cristina Lavorato and Pietro Argurio

Department of Environmental Engineering (DIAm), University of Calabria, Via P. Bucci, cubo 44/A, I-87036 Arcavacata di Rende, Cosenza, Italy; angela.severino95@gmail.com (A.S.); cristina.lavorato@unical.it (C.L.); pietro.argurio@unical.it (P.A.)

* Correspondence: raffaele.molinari@unical.it; Tel.: +39-0984-496699; Fax: +39-0984-496655

Abstract: Photocatalytic membrane reactors (PMRs) have been found to be very effective in the removal of organic pollutants (particularly recalcitrant compounds) from wastewater because they allow for the mineralization of organic pollutants to innocuous by-products, thus achieving high-quality treated water. Owing to the very high volumes of water involved, treated sewage wastewater could be reused if a very efficient tertiary stage, like a PMR, can be foreseen. In this review, the two main PMR configurations (photocatalytic membranes and slurry PMRs) were analyzed as requirements of a tertiary treatment of sewage wastewater considering six design and operational parameters of such plants: (i) continuous wastewater flow rate from the secondary stage; (ii) the self-control of the photodegradation rate related to wastewater chemical–physical parameters; (iii) ability to handle variations of wastewater concentration and flow rate; (iv) the control of the quality of treated wastewater; (v) low plant footprint; and (vi) easy maintenance. In this analysis, some characteristics of photocatalysis (which involves three phases: solid (the photocatalyst), liquid (the wastewater), and gas (oxygen or air)) and those of membranes (they can be produced using different materials and configurations, different processes (pressure-driven or not pressure-driven), etc.) were considered. The obtained results show that slurry PMRs seem more suitable than photocatalytic membranes for such applications. We believe this review can trigger a shift in research from the laboratory to industry in using photocatalytic membrane reactors.

Keywords: tertiary sewage wastewater treatment; photocatalytic membrane reactors; water reuse; heterogeneous photocatalysis; recalcitrant pollutants

Citation: Molinari, R.; Severino, A.; Lavorato, C.; Argurio, P. Which Configuration of Photocatalytic Membrane Reactors Has a Major Potential to Be Used at an Industrial Level in Tertiary Sewage Wastewater Treatment? *Catalysts* **2023**, *13*, 1204. https://doi.org/10.3390/catal13081204

Academic Editor: Carlos Vila

Received: 17 July 2023
Revised: 7 August 2023
Accepted: 9 August 2023
Published: 11 August 2023

1. Introduction

Currently, wastewater treatment plays a strategic role in mitigating the potable water shortage, so it is crucial for economic and health reasons, considering the worldwide population growth [1]. Acceptable water quality is required for discharge, reuse in the original production processes, irrigation, aquifer recharge, or other uses [2]. It has been widely demonstrated that conventional sewage (municipal) wastewater treatment plants (WWTPs) are inefficient in removing many pollutants, thus contaminating the receiving ecosystems [3–6]. These pollutants are mainly emerging organic contaminants (EOCs) that can have a lethal impact on human and wildlife endocrine systems, even if present in trace quantities. They include a diverse group of thousands of chemical compounds, such as pharmaceuticals and personal care products (PPCPs), pesticides, hormones, surfactants, flame retardants, plasticizers, and industrial additives, among others. Metabolites and intermediate degradation products of parent compounds [7,8] are also present, as well as two new classes of contaminants like antibiotic resistance genes (ARGs) and microplastics [9,10]. Another new class of contaminants particularly found in both drinking water and wastewater encompasses

polyfluoroalkyl substances (PFAs), which are persistent, mobile, and toxic chemicals that are hazardous to human health and the environment [11,12]. Many contaminants may undergo migration, transfer, transformation, degradation, and dissipation processes in the environment and may ultimately threat ecosystem and human health. Although WWTPs have a high pollution removal efficiency (e.g., over 95% in the case of microplastics [13]), resulting in low concentrations of these recalcitrant pollutants in the discharged water (e.g., from ng L^{-1} to μg L^{-1} for antibiotics [14]), the high daily flow rates (e.g., approximately 90,000 m^3/day in dry weather serving an equivalent population of 378,353 people [13]) leads to a considerably high number of pollutants that reach and accumulate into the environment. So, highly efficient wastewater treatment processes are required that include an advanced tertiary treatment stage to obtain water quality suitable for discharge but better for reuse purposes, thus fulfilling the aforementioned problems of potable water needs (the Food and Agriculture Organization (2021) expected the demand of water for irrigated agriculture to account for 70% of all freshwater withdrawals in the world by 2050 [15]). The current methods employed as tertiary stages, such as adsorption on active carbon and membrane filtration, are not able to destroy contaminants but only remove them via transfer to the adsorbent and the concentrate stream, respectively [16,17]. A promising alternative is the removal of persistent organic pollutants through destruction by means of advanced oxidation processes (AOPs), consisting of the action of powerful oxidants generated in situ, as well as reactive oxidizing species (ROS), e.g., hydroxyl radical ($HO^{\bullet}$) and superoxide radical ion ($O_2^{\bullet -}$) [18]. Among the different AOPs, those using heterogeneous catalysts have numerous advantages over types that have homogeneous catalysts [19], and among heterogeneous AOPs, those using semiconductor photocatalysts have shown to be an eco-friendly and sustainable alternative to overcome environmental and energy challenges [20]. Thus, photocatalysis is considered as one of the most promising advanced oxidation processes due to its ability to completely degrade contaminants to safer end products or intermediate compounds, its ability to handle a wide range of contaminants, having negligible requirement of post-processing, the disposability of spent stream, and mild temperature and pressure conditions [21]. In the most studied photoreactors for wastewater treatment, photocatalysts are used in suspended mode (slurry reactor) or immobilized on a support (fixed bed reactor). A slurry photoreactor offers a high surface area for reactions, but although it is more efficient than an immobilized system [22], there are some drawbacks such as (i) the difficulty of separating the photocatalyst at the end of a batch photocatalytic process; (ii) particle aggregation and agglomeration at high photocatalyst concentration; and (iii) the difficulty of operating a continuous process. On the other side, a drawback of immobilized photocatalysts is the efficiency of light impinging on particle surfaces, which is an important prerequisite for obtaining photocatalytic activity [23]. The difficulties related to photocatalyst separation as well as continuous operation for slurry photoreactors have been overcome around 2000, when several articles concerning the introduction of photocatalytic membrane reactors (PMRs) were published [24]. In a PMR, both photocatalytic reaction and catalyst separation occur, as well as continuous operation. In addition, since the membrane (if properly chosen) can be selective at molecular level, other than retaining the photocatalyst particles, the pollutant molecules can also be retained in the reaction zone until they are completely mineralized, resulting in improvement in the overall performance of the photodegradation process [25]. PMRs have been proposed and studied over the years in two main configurations: a photocatalyst suspended in a solution (slurry) retained by the membrane or immobilized in/on the membrane (photocatalytic membrane (PM) [26]). Under these two basic configurations, numerous sub-configurations have been proposed and tested for wastewater treatment, but none of them, to the best of our knowledge, have been deeply analyzed to understand if they fit the technical key parameters of a tertiary stage of a WWTP. Indeed, these plants usually operate with very high flow rates, continuous processing (night and day), and the presence

of numerous pollutants in solution. In this review, these operational characteristics, as well as those related to plant design (e.g., low footprint, robustness of operations, etc.) will be critically analyzed and related to the coupling of photocatalysis–membrane. Photocatalysis is a complex process as it not only involves three phases (solid (the photocatalyst), liquid (the wastewater), and gas (oxygen or air)) but also membrane operations (they can be carried out using different materials and configurations, different types of processes (pressure-driven or not pressure-driven), etc.). So, starting from the main characteristics of a tertiary stage of a WWTP, some main characteristics of a PMR in order to be employed as tertiary wastewater treatment will be identified and discussed. Then, some conclusions on possible PMR configurations that can be of interest for application at an industrial level will be drawn.

2. Technical Aspects of Tertiary Wastewater Treatment Technologies

Domestic and industrial wastewater systems are generally treated via the activated sludge process as the most widespread method. Although this process removes most of the organic content (which is converted into carbon dioxide and biomass), residual pollutants such as the previously mentioned emerging contaminants (ECs) will still be present, which have a significant impact on the final treated wastewater recipients [27]. Depending on the end use of the treated water, which could be its reuse, or it could be discharged into a water recipient, strict quality criteria need to be met [27]. The tertiary treatment methods that have gained significant research interest are chlorination, ultraviolet irradiation, membrane filtration, constructed wetlands, microalgae cultivation, ozonation, and photo-Fenton processes due to their low operational costs as well as their high efficiency. The most important technical efficacy parameter of these methods, namely the ability of each tertiary process to reduce pathogens and remove inorganic nutrients and ECs, was analyzed by Zagklis et al. [28], who found the photo-Fenton method to be the most technically efficient process, significantly reducing the microbial load and pharmaceutical content (by 4.9 log and 84%, respectively) of the secondary effluent. However, Lama et al. [19] provided evidence that AOPs based on the Fenton process have some drawbacks hindering their large-scale application. These include their narrow working pH range (2.5–6); the complexity of real water matrices favoring the precipitation of the transition metals present in the catalyst, leading to the formation of sludge; and undesirable by-products. Furthermore, the removal of soluble iron salts from the reacting environment requires extremely costly procedures. Some of these disadvantages related to Fenton- and photolytic-based processes can be mitigated using heterogeneous photocatalysis combined with membrane filtration [29–31]. The combination of these two technologies seems to be of particular interest in tertiary wastewater treatment as it has been successfully investigated in many published papers for achieving the comprehensive remediation of water streams [24,32]. The choice of the most appropriate tertiary treatment is a complex matter, since each method has certain strengths and weaknesses. Based on the requirements for the final quality of the treated water, it is possible to choose a combination in a multi-step process for the removal of target contaminants. Indeed, other than organic contaminants, nitrogen, phosphorus, and some metals could also be target components to be removed. However, in this review, we will only focus on the removal of organic contaminants in PMRs.

Tertiary treatment is performed in series after the secondary stage of a WWTP, so some of its technical characteristics are the same as those of the overall plant. In this review, we will consider the following design and operating parameters that different PMR configurations should also meet: (i) continuous wastewater flow rate from the secondary stage; (ii) the self-control of the photodegradation rate related to wastewater chemical–physical parameters; (iii) ability to handle variations in wastewater concentration and flow rate; (iv) controlling the quality of the treated wastewater; (v) low plant footprint; and (vi) easy maintenance.

3. Analysis of the Main Parameters of Tertiary Treatment and Requirements of the Corresponding Parameters of a PMR

The previously considered parameters, as the main technical characteristics of tertiary treatment, will be reviewed and analyzed in this section to relate them with the correspondent parameters of a photocatalytic membrane reactor.

3.1. Continuous Wastewater Flow Rate from the Secondary Stage

The fact that WWTPs operate continuously imposes a continuous operating mode for photocatalytic membrane reactors. This means that photodegradation reactions in the photoreactor must be carried out continuously (night and day) at a constant designed light intensity. Many studies on the applications of photocatalysis have highlighted the use of solar light as a green energy source, but solar light is available only during the day at a variable intensity [33]. So, to take advantage of the sunlight, photovoltaics [34] or other green sources (e.g., wind) generating electrical energy could be a valuable solution to reduce the consumption of electricity from the grid while continuously powering the lamps (e.g., low-energy-requiring LED lamps) for the irradiation of photocatalysts. This means that the exposure of photocatalysts to direct sunlight, as reported in some articles [35], is not of high interest when a continuous process is required.

Generally, WWTPs treat a thousand cubic meters of wastewater per day in small-scale plants, with flow rates ranging from about 50 to 1500 m^3/day, and this increases from medium- to large-scale plants [6]. In cases with significantly high flow rates, a criterion of modular designs can be followed by establishing a sub-plant size that is replicated n times until reaching the requested overall size, with these sub-plants operated in parallel. This criterion can be applied in designing a PMR after establishing its configuration.

3.2. Self-Control of the Photodegradation Rate Related to Wastewater Chemical–Physical Parameters

Common chemical–physical parameters of interest for wastewater are pollutants concentration, pH, and temperature. As reported in the Introduction, pollutants are various recalcitrant organic compounds that are still present in the effluent from the secondary stage of a WWTP. Their concentration is generally in the range of ng/L to µg/L. pH is generally in the range of 8.0–8.8, while the temperature for 75% of the world's global wastewater was estimated to fall into the temperature range of 6.9–34.4 °C over a year [6,36]. These parameters are also the operational parameters that influence the photodegradation rate of organic compounds.

For most photocatalytic reactions in the liquid phase, the photodegradation rate follows a kinetic model that is in very good agreement with the Langmuir–Hinshelwood (LH) model used to describe heterogeneous surface reactions [37]. Assuming LH kinetics for a generic photocatalytic process of degradation of species A, an expression for the initial reaction rate, r_A, is as follows:

$$r_A = k_{LH} \cdot \theta_A \cdot \theta_{Ox} \quad (1)$$

where k_{LH} is the second-order surface rate constant for the degradation reaction, which depends mainly upon the radiation flux, I; and C_A and θ_{Ox} are the fractional sites coverages by A and O_2 on the surface of semiconductor particles. The terms θ_A and θ_{Ox} are related to A and oxygen concentrations in a solution using the Langmuir model:

$$\theta_A = \frac{K_A C_A}{1 + K_A C_A} \quad (2)$$

$$\theta_{Ox} = \frac{K_{Ox} C_{Ox}}{1 + K_{Ox} C_{Ox}} \quad (3)$$

where K_A and K_{Ox} are the equilibrium adsorption constants, and C_A and C_{Ox} are the concentrations of A and oxygen, respectively.

The LH model states that the adsorption of the species on a catalytic surface is a rapid equilibrium process and that the slow rate-controlling surface step involves the presence of

both reactants (A and O_2) in a monolayer at the solid–liquid interface. Generally, in well-mixed photocatalytic systems, oxygen or air continuously bubbles, and the concentration of dissolved oxygen can be considered constant. Thus, Equation (1) can be rewritten as follows:

$$r_A = k'_{LH} \cdot \frac{K_A C_A}{1+K_A C_A}$$
$$\text{with } k'_{LH} = k_{LH} \cdot \frac{K_{Ox} C_{Ox}}{1+K_{Ox} C_{Ox}} \quad (4)$$

Tang et al. [38] studied the kinetics of the photocatalytic oxidation of five commercial dyes (Acid Blue 40, Basic Yellow 15, Direct Blue 87, Direct Blue 160, and Reactive Red 120) using TiO_2 under UV irradiation in a slurry reactor. They concluded that the different dyes follow the LH model at different pH values. At low pH, reduction using electrons in the conduction band may play a very important role in the degradation of azo dyes due to the reductive cleavage of azo bonds. In comparison, at neutral or high pH levels, hydroxyl radicals may be the predominant oxidation species. Oxygen plays an important role in the formation of hydroxyl radicals; in fact, its reaction with photoelectrons on photocatalysts' surface disfavors electron–hole recombination, and the superoxide ions formed ($O_2^{\bullet -}$) allow for a reaction channel for the generation of additional hydroxyl radicals through the formation of hydrogen peroxide [39–41], which occurs as follows:

$$O_2 + e^- \rightarrow O_2^{\bullet -}$$
$$O_2^{\bullet -} + H^+ \rightarrow HO_2^{\bullet}$$
$$HO_2^{\bullet} + e^- \rightarrow HO_2^-$$
$$HO_2^- + H^+ \rightarrow H_2O_2$$
$$H_2O_2 + e^- \rightarrow OH^{\bullet} + OH^-$$

Moreover, it is well known that the oxygen adsorption process on the photocatalytic surface is the rate-determining step for the kinetics of a photocatalytic reaction because it is much slower than H_2O and organic pollutants [42–44]. For this reason, a high oxygen concentration is used but a too-high oxygen concentration leads to competition with the reacting substrates for the adsorption sites [45]. Zhang et al. [46] used a metal-free nanotubular carbon nitride-based photocatalyst (CN NT) to activate O_2 under visible light for the degradation of organic contaminants. They observed that, when the N_2 flux increased from 0.02 to 0.1 L·min^{-1}, the degradation efficiency decreased from 71.5% to 62.3%. By contrast, when the O_2 flux increased from 0.02 to 0.1 L·min^{-1}, the degradation efficiency increased from 81.1% to 85.8%. Ma et al. [47] studied the degradation of pentachlorophenol (PCP) using TiO_2 under UV irradiation for investigating the role of generated ROS. They observed that $OH^{\bullet}$ played a dominant role in the degradation of PCP, whereas $O_2^{\bullet -}$ and H_2O_2 played a fundamental role in intermediates' degradation (Figure 1).

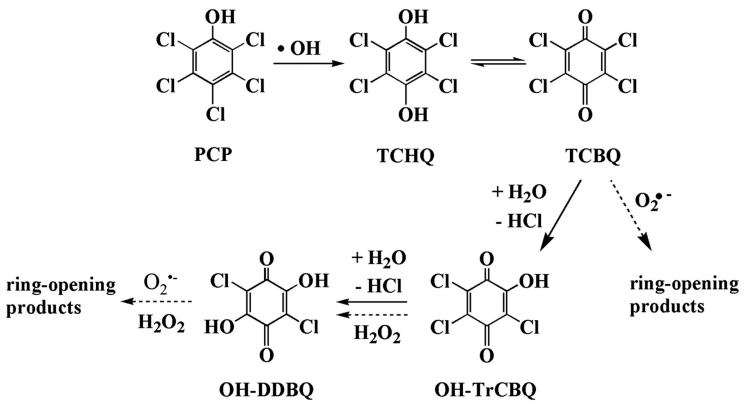

Figure 1. The proposed mechanistic steps in the photocatalytic degradation of PCP. Reprinted from [47]. Copyright (2019), with permission from Elsevier.

The pH of aqueous media is a key parameter that highly influences the charge at the surface and thus photocatalyst activity. Indeed, the position of band edges ($E_{c,s}$) is determined using the charge at the surface, that is, the potential drop in the Helmholtz layer (U_H):

$$E_{c,s} = E^0_{c,s} - qU_H$$

where $E^0_{c,s}$ is the position (on the energy scale) of the conduction band edge at the surface at $U_H = 0$, and q is the elementary charge. The Helmholtz double layer on semiconductors is typically determined through adsorption and desorption processes [48,49]. Therefore, due to pH, the charge on the semiconductor surface becomes positive or negative (Figure 2). The pH value at which the net surface charge is zero is called the isoelectric point (pH_{IEP}). If $pH > pH_{IEP}$, the surface is negatively charged, whereas if $pH < pH_{IEP}$, positive charges are present on the surface. This pH dependence of surface charge not only strongly influences the adsorption of charged or polarizable compounds but also determines the energetic position of the valence and conduction band, in other words, the thermodynamic feasibility of the interfacial electron transfer [37].

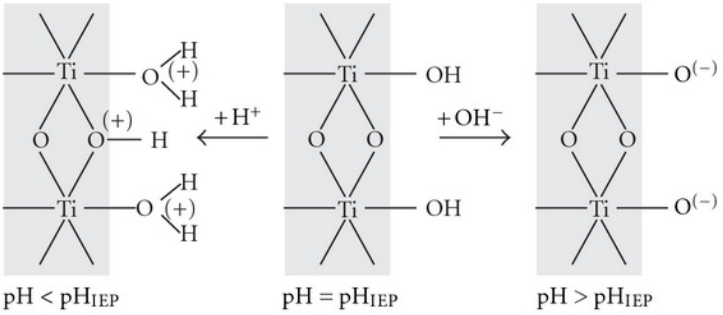

Figure 2. Scheme of the protonation and deprotonation of hydroxylated TiO_2 surface leading to positive and negative net charges at the surface, respectively. Reprinted from [48]. Copyright (2011).

The influence of pH on degradation was studied by Allè et al. [50], who verified the degradation of polymethylmethacrylate (PMMA) and polystyrene (PS) nanoparticles using TiO_2-P_{25}/β-SiC as photocatalyst under UV-A radiation. They found that degradation is faster at low pH (4–6) and a low flow rate [50]. Tan et al. [51] analyzed low-density polyethylene (LDPE) degradation using Design Expert software, which allowed for the interpretation of the association between pH, temperature, and catalyst (GO-ZnO) dosage. The optimum condition for the highest microplastic mass loss (39.47%) was pH 9.66, 30 °C, and 1500 ppm after 2 h of photodegradation. Minh Viet et al. [52] used La-TiO_2 under visible light for the photodegradation of phenol. They studied different pH values (4, 6 and 8) and found that the degradation performance of phenol enhanced from 61.3% to 98.2% by improving pH from 4.0 to 8.0, respectively. Ur Rahman et al. [53] studied the degradation of cefixime as an antibiotic model, using a CuO-NiO nanocomposite photocatalyst under sunlight. They observed that the degradation of cefixime was influenced by catalyst dosage and lower pH. Doong et al. [54] studied the influence of pH on the photocatalytic degradation of 2-chlorophenol using TiO_2 and found that a higher pH value had a significant effect. Indeed, they observed less formation of aromatic intermediates, suggesting that photodegradation at high pH favors direct ring cleavage. Mirzaei et al. [55] evaluated the photocatalytic degradation of sulfamethoxazole (SMX) using ZnO in the presence of fluoride ions (F-ZnO), studying the effects of operating parameters, and they observed that the removal of SMX was more efficient under acidic conditions and at an optimum pH of 4.8 since the surface fluorination of photocatalysts can be carried out in acidic media.

The above-described studies show that pH is an important parameter of photocatalytic reactions and that optimal pH can be different for different types of pollutants, but in a real process, only a pH value in the reacting zone can be imposed [56,57]. So, an optimal pH should be found for the overall pollutants present in wastewater. It is expected that pH

is around 8.5 (about the same as that of wastewater) where hydroxyl radicals may be the predominant oxidation species for the oxidation of various pollutants. This means that no or only little pH correction is required for the wastewater to be fed for tertiary treatment.

The temperature is also an important parameter; however, owing to photonic activation, photocatalytic systems can operate at room temperature. It is reported [37] that temperatures between 20 and 80 °C weakly influence the oxidation rate of photocatalytic reactions. This behavior can be explained by the LH mechanism described before. In fact, a decrease in temperature favors adsorption, which is a spontaneous exothermic phenomenon. However, the lowering of temperature also favors the adsorption of the final reaction products, whose desorption tends to inhibit the reaction [58,59]. Ariza-Tarazon et al. studied the impact of pH and temperature on the degradation process of high-density polyethylene (HDPE) using C, N-TiO_2, and visible light [60]. They observed that a low pH value allows for hydroperoxide formation during photooxidation and confirmed that low temperatures improved the degradation favoring the formation of microfractures on the surface. For this reason, low temperatures can facilitate oxidative degradation [61]. Gao et al. [62] prepared Ag@AgCl photocatalytic material based on calcium alginate as the carrier and cetyltrimethylammonium bromide as the surfactant (CA+) for the degradation of tetracycline under visible light. They studied the influence of temperature at 35, 40, and 45 °C and found that the highest photocatalytic degradation rate was at 40 °C. Maqbool et al. [63] used La-Mn co-doped Fe_2O_3 nanoparticles for the degradation of Rhodamine B (RhB) dye under a highly efficient solar light radiation. The degradation was optimized by changing pH (from 4 to 10), catalyst dosage (from 10 to 50 mg/L), dye concentration (from 10 to 60 mg/L), and temperature (35, 45, and 50 °C). They observed that the degradation of RhB dye increased from 43.30% to 89.34% as a result of the optimization of the system.

3.3. Ability to Handle Variations in Wastewater Concentration and Flow Rate

Depending on the type of photoreactor configuration, a better or a worse ability to handle variations in wastewater concentration and wastewater flow rate is expected. The basic reactor configurations operating in a continuous flow are continuous stirred tank reactors (CSTRs) and plug flow reactors (PFRs). CSTRs are mainly used in slurry photoreactors, while a PFR using immobilized photocatalytic systems is the fixed-bed photoreactor (FBP). The slurry–CSTR has the capability to mix solids, liquids, and gases simultaneously, while agitation increases the mass transfer between the catalyst and reactants, thus providing a high surface area to be illuminated. In fixed-bed photoreactors, photocatalysts are immobilized (fixed) on a material used as support. Although fixed-bed photoreactors do not require catalyst separation, light distribution has been a problem of concern [64,65]. Some examples of immobilized photocatalysts are the tubular membrane and the packed bed [33,66,67].

An increase in pollutant concentration in wastewater influences the photodegradation rate and thus the ability to mineralize the pollutants, which can require a greater residence time. An increase in the input flow rate, instead, reduces the residence time, thus decreasing the photodegradation efficiency. In the case of CSTRs, these variations are better mitigated (a well-mixed tank reduces the concentration pulse, while a slight increase in the hydrostatic level can reduce the flow rate pulse). The same does not occur for immobilized photocatalysts; thus, for wastewater treatment, it is speculated that a CSTR performs better than FBP. In these two basic configurations are also used photocatalytic membrane reactors. The membrane permits the confinement of the photocatalyst (slurry or immobilized) in the reaction zone and some types of membranes that are able to retain pollutants also facilitate the control of the residence time of some recalcitrant pollutants in the reaction zone [24]. A summary of various reactor configurations is reported in Figure 3 [65].

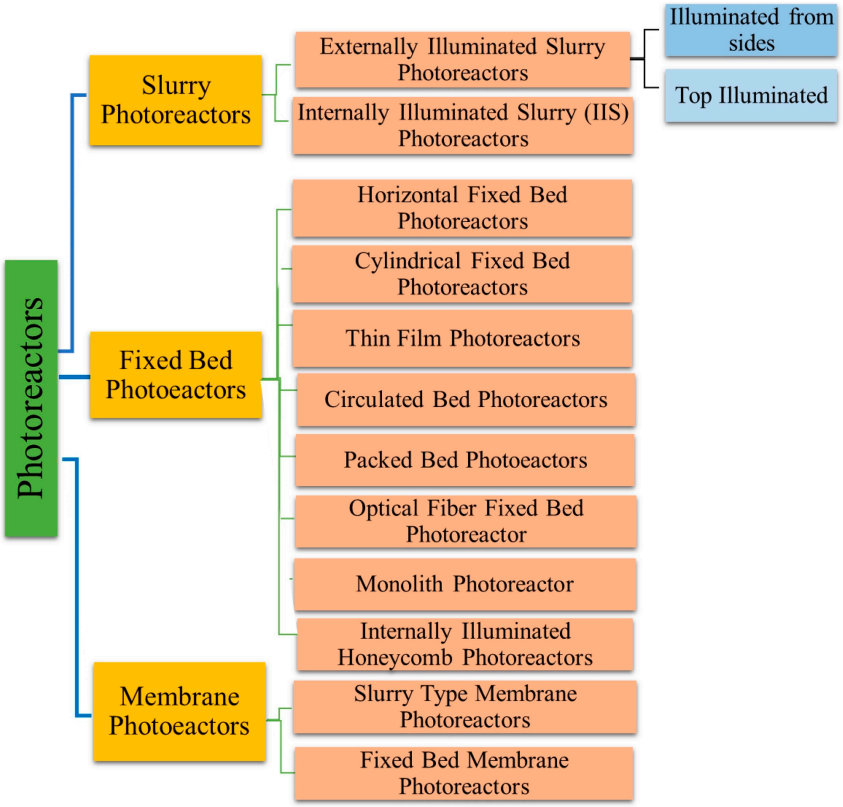

Figure 3. Classification of the main types of photoreactors. Reprinted from [65]. Copyright (2019), with permission from Elsevier.

In subsequent sections, an overview of some reactor configurations with or without membranes and the differences between these two systems are also described. This review of the literature can provide a significant amount of useful information to improve the design of membrane photoreactors.

3.3.1. Photocatalytic Reactor Configurations without Membrane

The performance of photocatalytic reactors can be influenced by their configuration [21]. The design of a photocatalytic reactor can include different configurations based on geometry, liquid agitation methodology (CSTR and stirrer rotation), light source (UV lamps and LED), bed dynamics (fixed bed and fluidized bed), and size (mini- and microreactors) [21,68,69].

Photocatalytic reactor design must address important parameters such as uniform light distribution, providing high illuminated catalyst surface area, and mixing inside the reactor [70]. The geometry of a photocatalytic reactor is important for maximizing the collection of the emitted light from the light source [71]. There are two main illumination configurations: external, in which the irradiation source is outside the reactor, and internal, with the lamp immersed in the liquid [71–74]. In both cases, this system can be built by using one or more lamps with different wavelengths (UV, visible, or solar light) and types of irradiation source (LED, Hg mercury lamp, etc.) [71,75,76] (Figure 4). Despite some advantages of using external illumination, such as the possibility of using direct solar irradiation as a light source and the easier reactor design, one possible limitation is the incomplete irradiation of the photocatalyst along the reactor's thickness. Instead, a system with internal illumination has the advantage of obtaining better contact with the photocatalyst surface, thus improving the overall performance of the photoreactor [24,77].

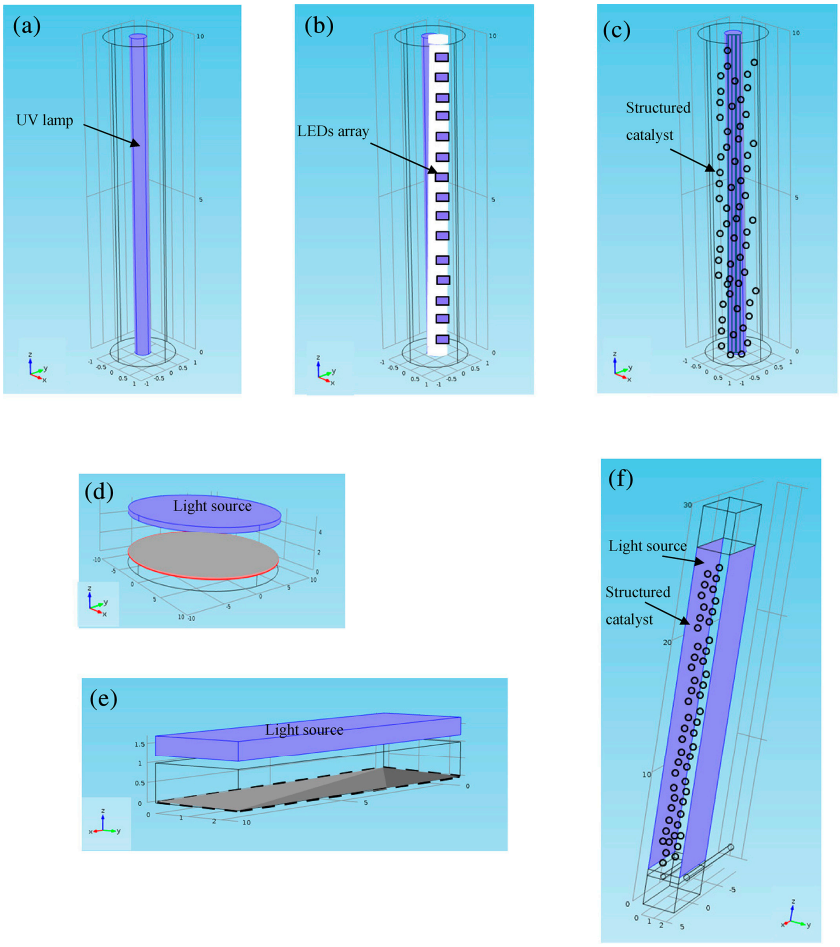

Figure 4. Examples of different photoreactor geometries: (**a**) annular geometry irradiated using a central lamp; (**b**) annular geometry irradiated using central light emitting diodes (LEDs); (**c**) annular packed-bed photocatalytic reactor; (**d**) parallel-plate disk photoreactor; (**e**) flat-plate photoreactor; and (**f**) flat-plate photocatalytic reactor filled with structured catalyst. Reprinted with permission from [71].

In the design of photocatalytic reactor configurations, it is very important to obtain a uniform light distribution in order to gain maximum effectiveness of the available catalytic surface [21]. To overcome this challenge, there is great emphasis on the use of multiple lamps, leading to the evolution of tube light reactors and multi-tube reactors [75,78,79].

Advances in artificial light sources (e.g., LED) have allowed for the design of compact UV reactors also including immobilized catalysts on substrates, such as glass fibers, optical fibers, and membranes [80–83]. LEDs can reduce operating costs and decrease the heat produced by standard lamps [84]. With respect to annular photocatalytic reactors, they have flat-plate geometry (Figure 4d–f), and they are scalable and usually employed if direct solar irradiation is used as a light source [71].

A particular method of photocatalyst irradiation is the controlled periodic illumination (CPI) in semiconductor photocatalysis, which is based on a series of alternate light and dark (TON/TOFF) periods [68]. A hypothesis suggests that upon the illumination of a catalyst, there is a critical illumination time during which absorbed photons generate oxidizing species (h_{vb}^{+}) on the surface of the photocatalyst. During an intermediate period in which the photons are not required, the generated species or their intermediates ($OH^{\bullet}$) react with substrates. This period does not need irradiation and should be conducted in the dark.

Another factor that should be considered is that the nature of the light source (solar or artificial) strongly impacts the design of a photocatalytic reactor [70]. Solar light, with relatively low intensity, needs a large exposed surface area, unless a solar concentrator

system (e.g., parabolic reflectors, Fresnel lens, and possibly optical fibers) is employed. In comparison, by using artificial light as a light source, it is important to optimize the conversion of electrical energy to useful photons in the most efficient way. Wang et al. [80] reported some designs of pilot- and full-scale photocatalytic reactors for water treatment (Figure 5).

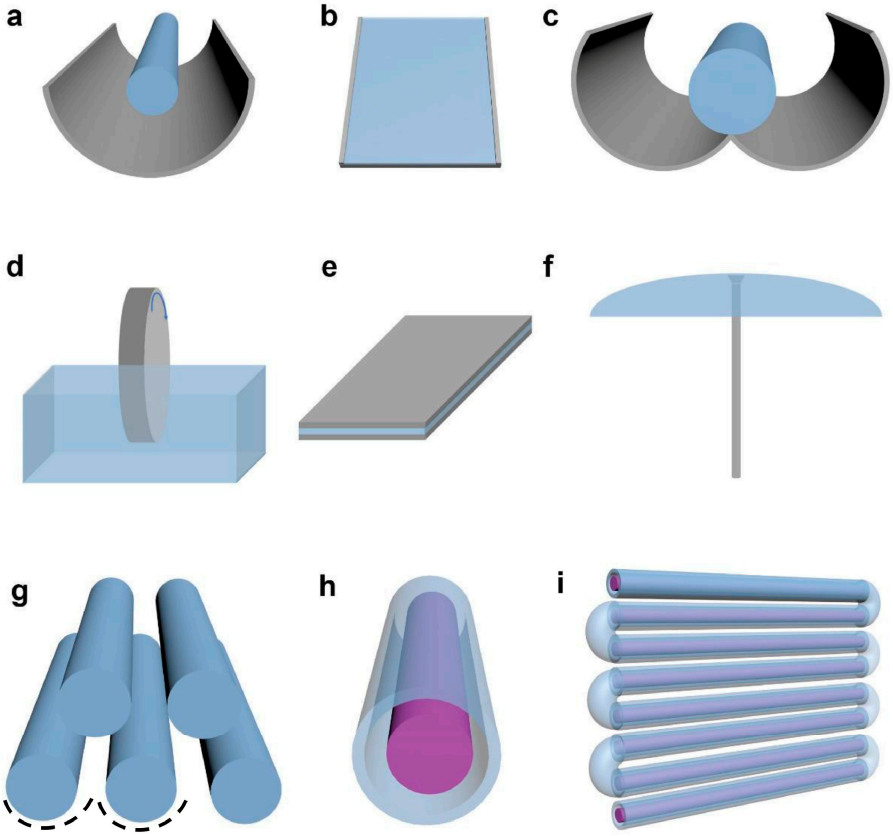

Figure 5. Geometries of several typical pilot-scale reactors for photocatalytic water treatment: (**a**) p parabolic trough reactor; (**b**) free-falling thin-film slurry reactor; (**c**) compound parabolic collector; (**d**) rotating disk or drum; (**e**) double-skin sheet reactor; (**f**) water bell fountain; (**g**) offset multi-tubular photoreactor; dash line shows that reactors are placed in a parabolic way; (**h**) annular thin-film slurry reactor mounted vertically; (**i**) serpentine assembly of annular thin-film slurry reactors. Reprinted from [80]. Copyright (2021), with permission from Elsevier.

Alpert et al. [85] reported one of the earliest pilot-scale solar photocatalytic reactors for water treatment built by Sandia National Laboratories (USA) (Figure 5a). This is a parabolic trough reactor used to treat hazardous wastewater containing trichloroethylene (PTRs), with a width of 2.1 m and length of 218 m, and a total aperture area of 465 m^2. To obtain maximum light absorption, this installation can control the orientation of parabolic troughs by tracking the sun's position by means of a motor. This system has different disadvantages, such as the absence of direct solar light during cloudy days and expensive water heating when required [86]. Figure 5b shows a free-falling thin-film slurry reactor system used by Gernjak et al. (2004) and Malato Rodríguez et al. (2004), which consists of a thin film of water flowing as a catalyst slurry or over an immobilized catalyst [87,88]. This system can collect both direct and diffuse solar light and, in general, does not require a sunlight tracking system, but its performance is affected by weather conditions and can induce catalyst sedimentation in slurry photocatalytic systems.

A type of photoreactor that is installed at a pilot scale to remove some micropollutants is the compound parabolic collector (Figure 5c). The compound parabolic concentrator (CPC) photoreactor is generally composed of a number of pyrex tubes connected in series

and irradiated using concentrated solar light transmitted with a parabolic round mirror, which allows for a concentration of sunlight equivalent to 25 or 70 suns, depending on the mirror area and aperture diameter [71,89]. By using compound parabolic collectors (CPCs), it is possible to capture both direct and diffuse components of solar light. They have turbulent flow regime operation and lesser dependence on weather conditions, do not overheat the water, and have a relatively small footprint [80,90]. A CPC plant with a solar collector field area of 150 m^2 for the removal of pesticides was installed in Spain [91].

Another type of configuration is the rotating disk photocatalytic reactor shown in Figure 5d [92]. Mehling et al. [93] recently described the use of a photocatalytic immersion rotary body reactor and a sub-stream ozonation as a fourth cleaning stage for its application in real wastewater. This photocatalytic immersion rotary body reactor with a 36 cm disk diameter, covered with stainless steel grids coated with titanium dioxide, was irradiated using UV-A light-emitting diodes. In this system, the concentrations of the generated radicals can be influenced by photon flux and ozone dosage, and the main limitation for the pollutant degradation rate is the layer thickness of water on the cyclically wetted rotating disks. Therefore, a further limitation of reaction rates should be expected through further scale-up processes for large-scale applications. Figure 5e shows a double-skin sheet reactor, which is simple in design and fabricated from a plexiglass double-skin sheet [21]. It provides better degradation efficiency than other reactors for a variety of contaminants and photocatalysts. A flat-plate reactor is a laminar flow reactor, which has less degradation efficacy, owing to limited solar radiation penetration at higher flow rates. Nevertheless, it produces better results than immobilized types in slurry-type reactors.

Another type of configuration is the fountain photocatalytic reactor (Figure 5f), which is a slurry-type reactor in which a thin film of polluted water containing dispersed photocatalyst is continuously generated by pumping water through a specially designed nozzle [94,95].

A configuration that can operate during both day and night with UV lamps inserted in the annular tube is the multi-tubular photoreactor (Figure 5g) [14,96]. Vaquez et al. reported the degradation of 14 antibiotics by using a tubular membrane photoreactor, operated in continuous mode and low residence times (from 3.9 to 12.2 s), in the treatment of demineralized water (DW) and secondary-treated urban wastewater (UWW) by using hydrogen peroxide (H_2O_2), persulfate ($S_2O_8^{2-}$), or ozone (O_3) as oxidant and titanium dioxide (TiO_2) or silver molybdate (Ag_2MoO_4) as photocatalysts [14]. In the UWW, by using O_3 as an oxidant, the removal of 12 antibiotics was higher than 90%; in contrast, by using $S_2O_8^{2-}$ with Ag_2MoO_4 as photocatalyst under UVC, the removal was higher than 60%.

Figure 5h shows a UV photocatalytic water treatment (PWT) unit that is an annular thin-film reactor, where slurry suspensions of TiO_2 are pumped to a liquid distribution system and falling freely along a vertically mounted hollow column with a UV lamp suspended in the middle of the hollow column through a quartz or borosilicate protective sleeve [80,97]. This configuration has the advantage of capturing almost all photons emitted by the light source; in addition, this typology of photoreactor is very efficient because the footprint is greatly reduced [98,99].

Another type of configuration (Figure 5i) is the serpentine-like geometry [100]. Mesa et al. [101] developed a UV PWT reactor with serpentine-like geometry that was tested in the treatment of effluents taken from handicraft factories by using a UV/H_2O_2 process and TiO_2-based photocatalysis. They obtained 70.80% of dye discoloration with 0.07 M of H_2O_2 and TiO_2 as photocatalysts.

3.3.2. Photocatalytic Membrane Reactors

Scientists started to realize the advantage of coupling heterogeneous photocatalysis with membrane processes in water and wastewater treatment around 2000, with the first studies on PMRs [102,103].

The main purpose of membrane use in PMRs is retaining photocatalyst particles and pollutant molecules in the reaction zone until they are mineralized, resulting in an improvement

in the overall performance of the photodegradation process. PMRs are commonly classified on the basis of photocatalyst arrangement in two main configurations [25]: (1) slurry PMRs, where the photocatalyst is suspended in the reaction mixture, and (2) PMRs with photocatalytic membranes (PMs), where the photocatalyst is immobilized in/on a substrate acting as a membrane [32,74,104]. Despite the advantage of immobilized photocatalysts over slurry systems, many studies have reported that slurry photocatalysts perform better than immobilized photocatalysts because they have larger active surface areas exposed to light [105]. Furthermore, Molinari et al. [106] reported that the use of a configuration with an immobilized photocatalyst on a membrane can cause the photodegradation of the polymeric membrane due to the presence of reactive oxygen species (ROS) in the oxidizing environment. Indeed, in this case, the membrane must be directly irradiated because pollutant degradation occurs inside the pores of the membrane or on its surface. For example, a PVDF membrane was used in various studies for immobilizing the photocatalyst [107,108], but in a study by Dzinun et al. [109], it was concluded that UV irradiation has some effect on the stability of the TiO_2/PVDF membrane within 30 days of exposure. Therefore, the use of polymeric membranes is limited for their low photostability and resistance against oxidative species, so a membrane material (e.g., inorganic membranes) with adequate stability against oxidative species under light irradiation should be used. Instead, the use of ceramic membranes can be preferred for their higher stability. Another disadvantage of PMRs with PMs is the lower rate of pollutant degradation with respect to slurry systems due to a lower mass transfer rate on the immobilized photocatalyst because the presence of support can limit the contact between the substrate and the photocatalyst. The first configurations of slurry PMRs, reported by Molinari et al. [110], were integrated systems based on the continuous recirculation of the slurry between the photoreactor (irradiated using an internal or external lamp) and the membrane cell that were operated in batch (recycling both the retentate and the permeate in the photoreactor) or in continuous mode by feeding the water into the photoreactor for treatment and withdrawing the permeate. A similar configuration with a hollow fiber ultrafiltration membrane (Figure 6) was investigated by Zhang et al. [111] in a photocatalysis–ultrafiltration process for dying wastewater treatment. They found that the rejection of dye in the presence of TiO_2 markedly decreased due to the deposition of TiO_2 particles on the membrane interface. So, the interactions between pollutants and photocatalysts and their effect on the performance of the membrane should be taken into consideration in this type of configuration.

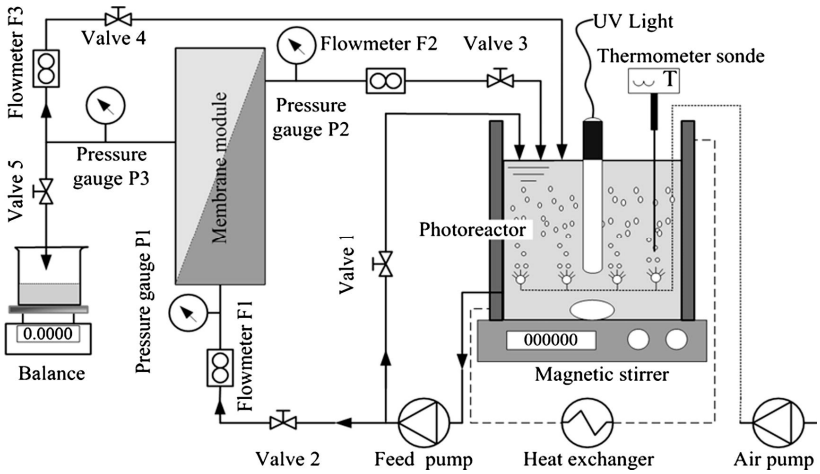

Figure 6. Schematic diagram of the experimental setup of a hybrid slurry photoreactor system with PAN hollow fiber ultrafiltration membranes. Reprinted from [111]. Copyright (2013), with permission from Elsevier.

Slurry PMRs can also be classified into two subcategories: (1) integrative-type PMRs, in which the photocatalytic reaction and membrane separation (MS) take place in the same vessel, where the inorganic or organic (polymeric) membrane is submerged in the slurry

photocatalytic reactor; (2) split-type PMRs, where the photocatalytic reaction and membrane separation take place in a photoreactor and membrane module that are appropriately coupled units [112–115].

PMRs can also be classified based on the placement of the light source: (1) PMRs with the light source above/inside the feed tank; (2) PMRs with the light source above/inside the membrane unit; and (3) PMRs with the light source above/inside an additional vessel placed between the feed tank and the membrane unit [25].

Although slurry PMRs achieve higher efficiency than that of PMRs with immobilized photocatalysts, there are two factors limiting their performance: (1) light scattering by the suspended photocatalyst nanoparticles (NPs); and (2) membrane fouling, with a consequent flux decline, caused by photocatalyst deposition on the membrane surface [78,102]. This last problem can be limited by using a membrane module with the correct selection of hydraulic conditions [116]. In general, membrane fouling can be reduced by using PMRs with PMs compared with conventional membranes because the photocatalyst generally makes the membrane more hydrophilic. To solve this problem, Molinari et al. [75] designed and built a new PMR configuration consisting of a slurry photocatalytic membrane reactor based on a vertical filter, working with gravity, and an external membrane that was tested in the photodegradation of a model pollutant in water. Figure 7 shows the configuration scheme of this PMR, in which the vertical filter is able to retain the photocatalyst, and the external nanofiltration (NF) membrane is able to retain pollutants in the photoreaction zone.

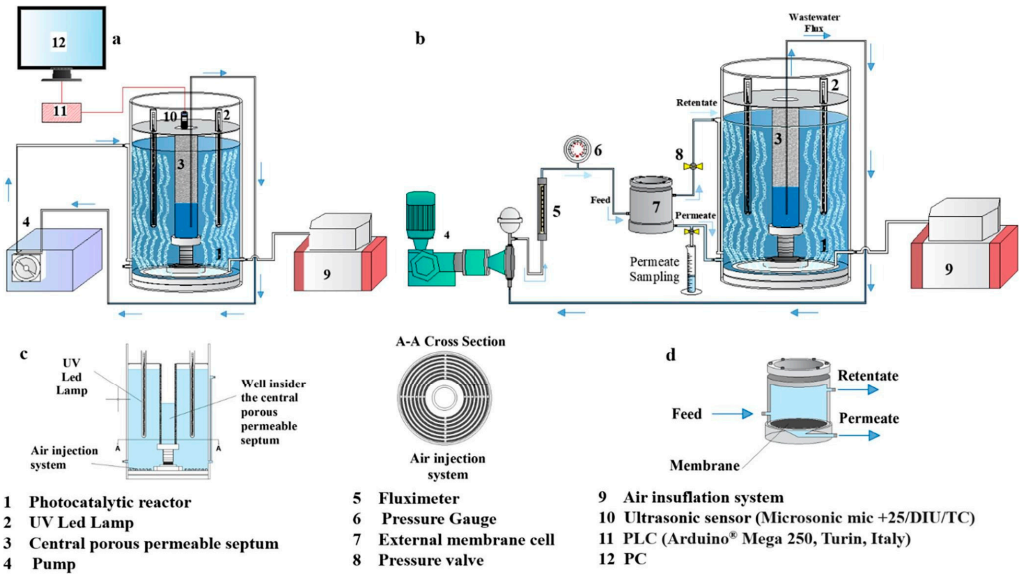

Figure 7. Scheme of a slurry PMR experimental setup with a vertical gravity filter and external membrane: (**a**) configuration used in hydraulic and photocatalytic preliminary tests; (**b**) complete slurry PMR configuration; (**c**) air injection system and cross-section; (**d**) cell containing the membrane. Reprinted from [75]. Copyright (2023), with permission from Elsevier.

The photocatalytic reactor shown in Figure 7 consists of a cylindrical plexiglass tank as the main unit with an external diameter of 24 cm and a height of 40 cm, with a maximum useful volume of 13 L inserted inside a cylindrical filter and four UV LED lamps [75]. Fixed at the bottom of the reactor, in the annulus area, there is a fine bubble air ventilation system (Figure 7c) consisting of a tubular polypropylene membrane circularly distributed over the entire surface to allow for setting appropriate mixing conditions and to provide the required oxygen for the photocatalytic oxidation of contaminants. The liquid was recirculated from the bottom of the well of the cylindrical filter to the external annulus (Figure 7a) using a tube connected to a pump that was used to feed the external membrane cell (Figure 7b). Some advantages of this type of configuration are (i) very reduced fouling via TiO_2 deposition in the external membrane cell because the vertical filter retains the photocatalyst, ensuring

greater flux than a submerged membrane (200 vs. 40 L m^{-2} h^{-1} average values); (ii) the easier replacement of the photocatalyst with a new one in comparison to a photocatalytic membrane; (iii) the external membrane (which is not exposed to light irradiation) facilitates recycling of non-photodegraded pollutants in the photoreactor, leading to higher quality of the treated water (permeate) than a submerged membrane. The membrane location is far from the strong oxidizing zone, thus preserving it from photodegradation and providing the possibility to use commercial spiral wound membranes with lower capital costs. The particles confined in the reaction zone and noncirculating in the membrane device, the very simple regeneration of the vertical filter, the use of low-energy LED-immersed lamps operating night and day using electrical energy (e.g., obtained via photovoltaic conversion of sunlight or other sources) are further advantages of this novel configuration. Researchers have reported 50% to 90% retention by changing the pH value, as well as 80% gemfibrozil degradation.

3.4. Control of the Quality of Treated Wastewater

The required final quality of the treated wastewater depends on its final use (discharge in water bodies, irrigation, aquifer recharge, etc.), but regardless, it needs to reduce the concentration of recalcitrant pollutants at the exit of the tertiary stage. Because different pollutants require different residence times for their mineralization, the presence of a selective membrane permits such a type of control acting at a molecular level. UF and MF membranes used to build photocatalytic membranes do not have such ability, so they will likely not result in good-quality treated water because not all pollutants will be mineralized with high efficiency in a continuous flow operation since, in this case, the residence time can not be controlled for all pollutants. Nanofiltration (NF) and reverse osmosis (RO) membranes, because of their ability to retain many organic pollutants, seem the most suitable to control the treated water's quality [117,118]. An RO membrane was tested in series to a submerged membrane to increase the quality of the treated water [119]. In some works, membrane distillation coupled with photocatalysis has also been found to result in high-quality treated water [120]. However, membrane distillation commercialization has been hampered by low flux performance (average flux of commercial membranes ~16 kg/m^2 h), while new carbon-incorporated membranes have higher flux performance (average flux of 47 kg/m^2 h), which shows the great potential of this membrane design [121]. However, the high energetic demand of MD represents a significant cost compared with pressure-driven PMRs [122].

3.5. Low Plant Footprint

When designing a plant, one criterion is the minimization of the consumption of soil, which means a low footprint. This objective can be reached by a proper choice of both operating conditions and plant components. For example, a low reactor volume is possible if the design permits a high reaction rate, which, in photoreactors, also depends on the irradiated photocatalyst surface. If direct solar light is used to irradiate the photocatalyst, a flat photoreactor allows for the maximization of the exposed surface, but this design has a higher footprint than a slurry photoreactor (aside from the problem of non-constant light intensity and light availability only during the day). With a simple calculation, this aspect can be evident. If we consider a slurry photoreactor of 1 m^3, the footprint can be, for example, 1 m^2 (if 1 m high is chosen) by irradiating the suspension with an appropriate number of immersed lamps. For flat photoreactors, if we hypothesize a light penetration depth of 0.1 m into the slurry, the 1 m^3 suspension volume is contained in a surface of 10 m^2, which means a 10 times higher footprint. Obviously, these values give only one idea of the differences between these two types of configurations. Indeed, the light penetration depth depends on the characteristics of aqueous media. In general, light intensity transmitted through a medium follows a logarithm decay according to the Beer–Lambert law. Light attenuation increases with the concentration of solute, the penetration depth, and the wavelength. In the case of pure water, negligible absorption has been observed in the wavelength range of 300–700 nm, while outside this range,

beam attenuation is observed [123]. However, for aqueous media, dissolved salts, organic substances, and suspended particulates result in beam attenuation, which is the sum of absorption and scattering phenomena. These considerations mean that we can only foresee a lower slurry reactor footprint than a flat photoreactor, but the extent of the difference can be determined with measurements on related pilot plants in a real environment.

Other parameters that influence the footprint of membrane photoreactors are (i) the reaction rate of immobilized and suspended photocatalysts; (ii) light source, light intensity, and wavelength; and (iii) membrane configuration.

3.5.1. Reaction Rate of Immobilized and Suspended Photocatalysts

As already reported, two basic photoreactor systems, namely the suspended configuration and the supported photocatalyst configuration, have been studied. A suspended photocatalyst system is generally more efficient than a supported system due to its larger surface area. It is crucial that all photocatalyst particles are illuminated, but this does not always happen in suspended systems because the particles further away from the light source are hidden from the radiation by the particles near the light source (although good mixing reduces this drawback, as will be discussed later). A solution to this problem could be the use of an immobilized system where the photocatalyst is placed as a layer, and all particles are illuminated. However, the mass transfer is limited, only a part of the photocatalyst is in contact with the solution, and illumination is always achieved on the same side of the particle surface, meaning that if this is fouled, the other part of the surface cannot be used [124,125]. Slurry systems do not have these drawbacks. Manassero et al. [126] tested three different reactor configurations: a slurry reactor, a fixed-film reactor with TiO_2 immobilized onto the reactor window; and a fixed-bed reactor filled with TiO_2-coated glass rings. Their performance was assessed considering two parameters: (1) the photonic efficiency, which is the ratio of the reaction rate to the rate of incident photons; and (2) the quantum efficiency, which is the ratio of the reaction rate to the photon absorption rate (Figure 8). The results show that the slurry reactor was the most efficient configuration, and the fixed-bed reactor had a value of quantum efficiency only one-third lower than the suspended system.

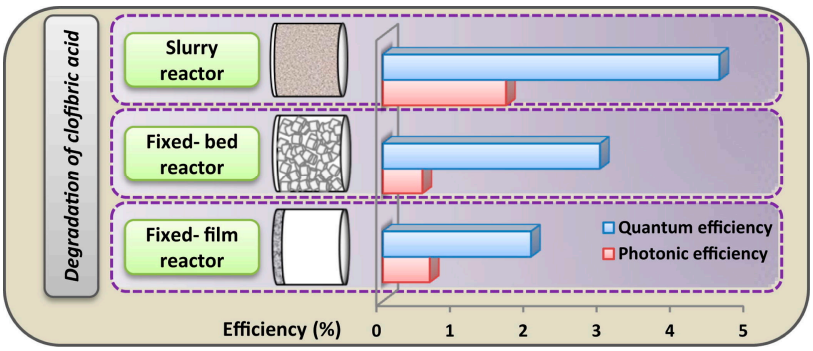

Figure 8. Comparison of three different reactor configurations (slurry, fixed-bed, and fixed-film reactor) considering photonic efficiency and quantum efficiency. Reprinted from [126]. Copyright (2017), with permission from Elsevier.

The support (carrier) materials used for immobilizing the photocatalyst must meet certain requirements, which can be distinguished into two groups. The first group includes stability, reusability, environmental aspects, and the cost of preparation. The second group includes the influence on photoelectrochemical reactions, considering better light harvesting, less charge loss, and more contact between the adsorbed pollutants' molecules and the photogenerated ROS [127]. An example of an immobilized photocatalyst is presented in the research of Uheida et al. [128], in which a new approach was used for the degradation of microplastics (MPs) like spherical particles of polypropylene (PP) suspended in water via the visible light irradiation of zinc oxide nanorods (ZnO NRs) immobilized onto glass fibers. After two weeks under visible-light-led irradiation,

they obtained a reduction in the average particle volume by 65%. Shen et al. [129] used a Bi_2WO_6 photocatalyst coated on silica sands for the degradation of sodium isobutyl xanthate (SIBX) under visible light irradiation, in a continuous fixed-bed photoreactor. The maximum degradation percentage reached 95.40% after 70 min of visible light irradiation under optimal conditions. Ljubas et al. [130] degraded trimethoprim (TMP) using a nanostructured TiO_2 film on a glass ring at the bottom of a reactor under a solar radiation lamp, and they observed the complete degradation of TMP in ultrapure water after 3 h.

As regards slurry photoreactors, Molinari et al. designed a submerged slurry photocatalytic membrane reactor able to retain pollutants (gemfibrozil) in the photoreaction zone, where the TiO_2 photocatalyst is present under UV irradiation [75]. They observed an 80% reduction in initial concentration after 4 h. In another study [131], using a slurry reactor with 1200 mg L^{-1} of H_2O_2 (solution 25 wt%) under UVC irradiance of 31.8 mW cm^{-2}, Easton et al. obtained a 26.6% of mass loss of microplastic polyethylene terephthalate after 9 h of irradiation. García-Muñoz et al. [132] studied the degradation of different sizes of polystyrene (PS) nanoplastics in water by using both slurry and immobilized reaction modes and TiO_2 as a photocatalyst. From an analytical point of view, they observed that an immobilized photocatalyst poses fewer analytical problems, owing to the absence of photocatalyst microparticles in the samples compared with a slurry reactor.

Aside from the above results on immobilized and suspended photocatalysts, an important point for application is their kinetic difference because this has an impact on the plant footprint. Indeed, the higher the reaction rate, the lower the reactor footprint. In Table 1, a comparison between the reaction rate of the same photocatalyst in immobilized and suspended forms is reported.

Table 1. Comparison of the reaction rate of the immobilized and suspended (slurry) photocatalyst.

Photocatalyst	Pollutant	Slurry	Fixed-Bed	Results	Kinetic Constant (*)	Ref.
GCN-T	Metoprolol and venlafaxine	1 g L^{-1} of GCN-T	GCN-T immobilized in the form of a film (GCN-T/PVDF) of 30 cm^2	100% pollution removal after 180–240 min using the GCN-T/PVDF film and after 30–60 min using the GCN-T powder	k^i_{app} were 0.766 min^{-1} and 0.879 min^{-1} for 0.90 µM and 0.065 min^{-1} and 0.056 min^{-1} for 90.1 µM of metoprolol and venlafaxine, respectively	[133]
TiO_2	50 mg L^{-1} phenol	bubbling air, 300 mg L^{-1} TiO_2	The glass plates (4.5 cm × 4.5 cm × 3 mm) were prepared with 0.10 ± 0.01 g of catalyst	Significant catalyst deactivation was observed in the immobilized-catalyst systems	k^s_{app} = 0.0013 min^{-1} k^i_{app} = 0.0010 min^{-1} After 24 h of reaction k^i_{app} was 60% of its initial values	[134]
TiO_2	20 mg L^{-1} of clofibric acid (CA)	0.5 g L^{-1} of TiO_2 in a solution saturated with pure oxygen	TiO_2 supported on the illuminated reactor window (fixed film reactor, FFR) with a mass of 36.5 mg, and TiO_2 immobilized over the surface of glass rings used to fill the reactor (fixed bed reactor, FBR) with a mass of 21.2 mg	The slurry reactor was the most efficient configuration, the fixed-bed reactor gave a value of quantum efficiency only one-third lower than the suspended system	k^s_{app} = 3.26 × 10^3 min^{-1} k^i_{app} = 1.12 × 10^3 min^{-1} (fixed bed reactor) k^i_{app} = 1.28 × 10^3 min^{-1} (fixed-film reactor)	[126]

Table 1. *Cont.*

Photocatalyst	Pollutant	Slurry	Fixed-Bed	Results	Kinetic Constant (*)	Ref.
TiO_2	100 μg L^{-1} of 15 emerging contaminants (ECs)	5 mg L^{-1} of TiO_2	The photoactive layer of TiO_2 was deposited on glass spheres using the sol–gel dip-coating technique. Around 0.5 mg of TiO_2/sphere	The removal percentage was between 100% in most of the compounds and 70% of the sulfamethoxazole and atrazine. The degradation rate in the TiO_2 slurry was similar at low concentrations	Ofloxacin: k^i_{app} = 1.577 min^{-1} and k^{5i}_{app} = 0.228 min^{-1}, Flumequine: k^s_{app} = 0.141 min^{-1} and k^i_{app} = 0.46 min^{-1}), Hydroxybiphenyl: k^s_{app} = 0.025 min^{-1}, k^i_{app} = 1.577 min^{-1} and k^{5i}_{app} = 0.047 min^{-1}	[135]
TiO_2	200 mg L^{-1} of trichloroethylene (TCE)	0.2% wt/wt TiO_2	72 g of TiO_2 films containing 1.4 wt% of TiO_2 added to reactor	The operation of the solar light/TiO2 slurry and immobilized systems showed 100% (TiO_2 slurry system), 80% (TiO_2 immobilized system) degradation of the TCE after 6 h	k^i_{app} = 0.0052 min^{-1} k^s_{app} = 0.0224 min^{-1} (with H_2O_2) k^i_{app} = 0.0083 min^{-1} (with H_2O_2) k^s_{app} = 0.0304 min^{-1} (with $S_2O_8^{2-}$) k^i_{app} = 0.0207 min^{-1} (with $S_2O_8^{2-}$)	[136]
ZnO	Carbamazepine (CBZ)	0.5 g L^{-1} of ZnO nanoparticle suspensions and 10 mgL^{-1} of CBZ	10 μmol L^{-1} of CBZ and 0.5 g L^{-1} of ZnO (nanoparticles grafting onto inert foam substrates)	The photocatalytic degradation of CBZ was 67% after 4 h using the foams	$k^s_{app} = 3.3 \times 10^{-3}$ min^{-1} $k^i_{app} = 3.0 \pm 0.4 \times 10^{-3}$ min^{-1} (foams sintering at 900 °C for 6 h) $k^i_{app} = 3.2 \pm 0.2 \times 10^{-3}$ min^{-1} (foams sintering at 1000 °C for 12 h)	[137]
TiO_2	10 or 40 mg L^{-1} of 4-nitrophenol (4-NP)	0.5 g L^{-1} of suspended TiO_2	Amounts of immobilized TiO_2 were 0.76, 2.04, 4.08, and 6.12 mg/cm^2 of polymeric membrane	51% *w*/*w* of 4-NP was removed after 5–6 h of operation in the immobilized system and 80% *w*/*w* of 4-NP degradation was obtained in 5–6 h of operation in the suspended system	k^s_{app} = 0.27 h^{-1}	[106]

Table 1. *Cont.*

Photocatalyst	Pollutant	Slurry	Fixed-Bed	Results	Kinetic Constant (*)	Ref.
TiO_2 (P25)	10^{-3} M of 3,5-dichlorophenol (3,5-DCP)	1625 ppm of P25	TiO_2 nanocrystalline thin films were developed on glass substrates by applying dip coating and doctor-blade deposition techniques with a surface area of 0.8 cm^2	Complete degradation of 3,5-DCP occurs in less than 100 min using the slurry system, with the doctor-blade TiO_2 films achieved after about 360 min of illumination and for the sol–gel films after about 1600 min	k^i_{app} = 0.0079 min^{-1} and 0.0023 min^{-1} for Optical Fiber/TiO_2 Coating and Optical Fiber/TiO_2 sol–gel-coated, respectively	[138]

(*) k^i_{app} is the apparent kinetic constant of the immobilized photocatalyst; k^s_{app} is the apparent kinetic constant of the slurry photocatalyst; k^{5i}_{app} is the apparent kinetic constant of the immobilized photocatalyst after five cycles. In all three cases, pseudo-first-order kinetics was considered.

3.5.2. Light Source, Light Intensity, and Wavelength

The minimum radiation wavelength required to promote an electron from the valence to the conducting band of a semiconductor depends upon the bandgap energy of the photocatalyst. When a photon of a certain wavelength impinges on the photocatalyst surface, if the energy is equal to or greater than the bandgap value, electrons are moved from the valance band and transferred to the conducting band. This leaves positive holes in the valence band, which, in the presence of O_2 and H_2O, generate $OH^\bullet$ radicals, the most potent oxidizing agents, leading to the destruction of pollutants [139]. The species formed are named ROS, which in addition to hydroxyl radical ($OH^\bullet$), also include superoxide radical anion ($O_2^{\bullet-}$) and H_2O_2. The most dominant ROS is the hydroxyl radical, which, despite its rather short lifetime (approximately 10 μs in natural water), is the most oxidant species [47]. When a semiconductor is present as a powder in suspension, each particle acts as a small photocell, and in 100 mg of powder, consisting, for example, of 0.1 mm diameter particles, more than 10^{11} independent particles are present, thus making the system very effective [37]. The incident light that initiates the photocatalytic reaction is in a wavelength region that is absorbed by the photocatalyst [140]. The minimum wavelength required to promote an electron depends upon the physicochemical properties of the photocatalyst [141]. Many synthesized photocatalysts have different bandgap energy values, and for this reason, the optimization of the light source is an important parameter. Generally, for UV irradiation, UV lamps are used, but the use of this type of lamp has some disadvantages like fragility, toxicity (due to mercury), short lifetime, high-energy consumption, etc. [142,143]. Alternatively, over the last few years, light-emitting diodes (LEDs) have opened a new path for their low energy consumption [144]. However, the use of UV-LED is still under debate, with researchers discussing whether ultraviolet light is enough for photocatalysts and questioning the proper frequency range to be used during the oxidation process. Nevertheless, there are some advantages to the use of LEDs such as reduced costs, compact size, lightweight, lower operating temperature, long lifetime, the possibility of operating night and day, and choice of the number and position of the lamps inside the photoreactor to optimize the reaction rate and thus the reactor's footprint. With the development of UV-LED technology, it is possible to pulse UV-LEDs thus conducting controlled periodic illumination (CPI) [145], as already described in Section 3.3.1. CPI is characterized by a period of light-on and light-off. CPI application allows us to have an optimal number of photons a photocatalyst can utilize in a given turnover number (T_{ON}) period or under continuous illumination before saturation. Pulsed LED light allows for the enhancement of the efficiency of a photocatalytic reaction, thus facilitating the determination of the specific light intensity required for improvement in the photonic efficiency [68]. In particular, it is known that, at low light intensity (0–20 mW/cm^2), the reaction rate increases linearly

with light intensity (first order); in contrast, at intermediate light intensities (25 mW/cm^2), the rate depends on the square root of the light intensity [146]. The increase in light intensity allows for electron–hole formation as well as their recombination, while at a low light intensity, electron–hole formation is predominant, and recombination does not occur. When the light intensity is increased, electron–hole for degradation will compete with electron–hole recombination [147]. Liang et al. [148] used pulsed UV-LED with modulation for TiO_2 irradiation in an advanced oxidation process for the degradation of pharmaceutical micropollutants. They observed that when TiO_2 is immobilized on a substrate and irradiated using UV-LEDs, the use of CPI is determining. Sannino et al. [149] studied the impact of light modulation on the decolorization of Acid Orange 7 (AO7), using a fixed-bed photocatalytic reactor containing a N-TiO_2 photocatalyst under irradiation by visible light generated using 240 white LEDs. The system was optimized with a current between 50 and 100 mA, a period of 10 s, and a sinusoidal modulation.

3.5.3. Membrane Configuration

The low footprint of photocatalytic membrane reactors is related also to membrane configuration. If a membrane reactor is based on photocatalytic membranes (which means immobilized photocatalysts in various configurations), the irradiation of the photocatalytic layer requires maximizing the exposed surface area, which means a higher footprint than a CSTR–slurry photoreactor, as estimated at the beginning of this section. For CSTR–slurry photoreactors, the most studied configuration is that with a submerged membrane where the permeate is sucked with a pump. In applications different from photocatalysis, a recent approach that does not use a pump to withdraw the permeate is the use of a gravity-driven membrane, which is subject to the phenomenon of flux stabilization and requires less energy consumption [150,151]. A gravity-driven membrane that could be of interest for photoreactors at the industrial level is the submerged flat plate that was used in a membrane bioreactor (MBR) in a case study by Toray. The membrane had pores of a nominal size of 0.08 μm (between ultrafiltration and microfiltration) and the average flux was 25.7 LMH (L m^{-2} h^{-1}); the filtration method was via gravity; the total membrane area per module was 560 m^2 in a double-deck arrangement, with 10 modules and 144 m^3/h total capacity; and system footprint required 12 m of length and 4 m of width for the membrane tank [152]. However, as already reported by Molinari et al. [75], ultrafiltration and microfiltration membranes do not have a high capacity to retain many pollutant molecules, so, if a high quality of treated water is required, nanofiltration (NF) or reverse osmosis (RO) membranes must be used to treat the permeate from MF or UF. In that work, an NF membrane was used, and instead of a submerged membrane, a vertical filter working with gravity was used. In this configuration, the plant footprint, aside from the photoreactor, is related to NF or RO membrane configuration. The spiral wound module is the most used for NF and RO operations in plants with a water processing capacity of thousands of cubic meters per day, due to its high packing density (membrane surface per unit volume), high-level of salt rejection and water permeation, and flexibility of scale-up (ranging from a small size to large size) [153,154]. In choosing the type of spiral wound module, the feed spacer is of particular interest because it influences the performance of the module [155]. It is foreseen that these types of modules (NF and RO), which are commercially available with different characteristics (membrane material, rejection, flux, feed spacer, etc.), can contribute to improving the water quality obtained from a PMR as well as a reduction in plant footprint.

The use of a suitable selective membrane also contributes to reducing the plant footprint by controlling the residence time in the slurry–CSTR to achieve the maximum mineralization of the various pollutants. Indeed, the rejection ability of the membrane to retain many pollutants in the reaction ambient until they are mineralized allows for the design of the photoreactor volume by considering only the minimum retention time (RT = V/Q, where V is the reactor volume, and Q is the incoming flow rate). Since different pollutants need different retention times to be mineralized, the slurry–CSTR system combined with

RO or NF has a significant advantage over conventional photoreactors and photocatalytic membranes (these usually operate in a flow-through mode). In these last two cases, the size of the reactor volume must be determined using the highest retention time, meaning a high volume (and thus a high footprint) if Q is fixed.

3.6. Easy Maintenance

Each industrial plant requires accurate engineering actions during the life cycle, allowing for restoring the system to a state of functionality and, eventually, improving its functionality if the upgraded components of the plant will be available. These components include, for example, a new photocatalyst with improved performance, new types of lamps, new membrane modules, etc. If the plant has been designed with a criterion that allows for easy acquisition of new functionalities, this could be very relevant. For membrane photoreactors, a component that could require adjustment during the plant life cycle is the photocatalyst. Depending on the confinement mode of the photocatalyst (slurry confined by the membrane or immobilized in/on a membrane), the difficulty of adjustment can be significantly different. This could concern (i) the amount and type of photocatalyst, and (ii) photocatalyst deactivation and regeneration, as described in the following section.

3.6.1. Amount and Type of Photocatalyst

The photocatalytic effect is related to the bandgap value of the photocatalyst, which enables the chemical reaction [156]. The initial step for heterogeneous photocatalyst systems is photonic excitation on the catalyst surface. Therefore, the reaction rate depends on the amount and type of photocatalyst. In fact, it is known that, after a certain value of photocatalyst mass, the reaction rate levels off and becomes independent of mass. This limit depends on parameters such as geometry, the working conditions of the photoreactor, and the mechanism of the photocatalytic reaction that promotes the formation of $OH^{\bullet}$ radicals and substrate adsorption on the catalyst surface. High quantities of photocatalysts cause a screening effect, which masks part of the photosensitive surface, and thus leads to a reduction in $OH^{\bullet}$ radical generation, which reduces photocatalytic activity [58,75,157]. However, some scattering from directly irradiated particles to some indirectly irradiated particles can occur, thus reducing the masking effect. This phenomenon mainly occurs in slurry photocatalysts rather than in immobilized photocatalysts.

It is also important to define the correct type of photocatalysts for water pollution degradation. Cao et al. compared different catalysts for polystyrene (PS) degradation such as TiO_2, ZnO, ZnS, and g-C_3N_4 [158]. From this study, they observed that TiO_2 is the worst for polystyrene degradation. In comparison, for different antibiotics, Habibi et al. highlighted the impressive activity of a CeO_2-x/$AgFeO_2$/Ag photocatalyst [159]. Bismuth sillenite crystals were studied by Baaloudj et al. for water treatment [160]. Carbon material in various forms (nanoporous carbon, nanotubes, etc.) as a dopant on TiO_2 was reviewed by Mestre and Carvalho for the photodegradation of various recalcitrant pharmaceuticals in wastewater [161]. Photocatalytic adsorbents like Fe/Mn-SiO_2 nanocomposites and Fe-AC (activated carbon) were studied by Baek et al. [162] in the photocatalytic degradation of pharmaceuticals and perfluorinated compounds in an aqueous environment. Qanbarzadeh et al. [163] used a boron nitride photocatalyst to efficiently degrade poly-/perfluoroalkyl substances in complex water matrices. These examples show that research on new and more active photocatalysts is of broad interest. Furthermore, bare photocatalysts can be limited by their wide bandgap, which requires higher energy of incident light, resulting in a response region only in the ultraviolet light. For this reason, it is of interest to consider some approaches that promote charge separation and light utilization like support presence, metal loading, doping nonmetallic element, and decorating with functional group [164]. Packialakshmi et al. [165] synthesized ZnO/SnO_2/reduced graphene oxide nanocomposites (ZnO/SnO_2/rGO NCs) for the photocatalytic degradation of organic dye pollutions. The use of ternary nanocomposites (NCs) provides different properties, such as crystallinity, low recombination of photogenerated charge carriers, energy gap, and surface morphologies. They compared photocatalysts like ZnO, ZnO/rGO, SnO_2/rGO sam-

ples, and ZnO/SnO_2/rGO NCs. They found that nanocomposites had great photocatalytic effectiveness for the destruction of orange II (99.8%) and reactive red 120 dye (97.02%), after 120 min of sunlight irradiation. Gordanshekan et al. [166] degraded Cefixime (CFX) using Bi_2WO_6/g-C_3N_4 (BC mass ratio of 60%) and Bi_2WO_6/TiO_2 (BT mass ratio of 12.5%) under UV–visible light irradiation. After 180 min of reaction, CFX and the by-products were entirely mineralized. The LC-MS and TOC tests revealed that most toxic products were not present after 135 min of reactions. Leelavathi et al. [167] synthesized a ternary g-C_3N_4/Co/ZnO heterojunction photocatalyst for methylene blue (MB), crystal violet (CV), and rhodamine B (RhB) degradation, and degradation rates of 96.3%, 74.5% and 75.14%, were observed, respectively. RhB was irradiated under visible and sunlight, and the degradation efficiency increased to 91.6% under sunlight. Maulana et al. [168] used Ag/TiO_2 for the degradation of polyethylene (PE); in particular, they studied different microplastic range sizes, namely 100–125, 125–150, and 150–200 µm. Their results showed that, at an initial concentration of 100 ppm, the best degradation percentage at particle size 125–150 µm was 100%, which was achieved at 90 min irradiation. Denisse et al. [169] synthesized C,N-TiO_2 and tested the purification of 50 mL solution with a 2 wt/vol% aqueous dispersion of polystyrene (PS) and 0.01 wt/vol% aqueous dispersion of PS in a batch-type glass reactor. They studied the calcination treatment of the photocatalyst at different temperatures and found that the TiO_2-based photocatalyst can be a good candidate for polystyrene degradation but not enough to achieve high degradation efficiency.

The choice of the type of photocatalyst for tertiary wastewater treatment is also related to the pH range where the photocatalytic activity is high. Indeed, as already reported, the pH of the wastewater that feeds the tertiary stage (PMR in our case) is around 8.5, and it is not conceivable to change it because of the very high wastewater flow rate. This prompts the use of photocatalysts with maximum activity in a wide pH range with an average value of 8.5. For example, in the study of Despotovic et al., using ZnO nanoparticles, the apparent kinetic constant was higher in the pH range 7–10 for the drug amitriptyline, while for the pesticides clomazone and sulcotrione, it was independent of pH [170]. In another work, the photocatalytic degradation of sulfamethoxazole was carried out at pH 4.7 on ZnO and TiO_2 (P25) photocatalysts [55]. Despite the interesting results from a scientific point of view, these last data are of no interest for sewage WWT because the working pH (4.7) is outside of that of interest (8.5 as the average value).

A further aspect that can limit the development of photocatalytic reactors in sewage WWT, and PMRs in particular, is the availability of massive quantities of photocatalysts as well as the availably of photocatalyst mixtures. Indeed, it can be foreseen that a mix of photocatalysts could perform better than a single photocatalyst because, from the existing literature, it has been widely observed that various pollutants are photodegraded with different rates on the same photocatalyst. This means that research should be conducted by testing real wastewater (or mixtures of many pollutants) and different mixtures of photocatalysts.

3.6.2. Photocatalyst Deactivation and Regeneration

Many studies have highlighted the potential of photocatalysts such as ZrO_2, SnO_2, Fe_2O_3, WO_3, CeO_2, ZnS, TiO_2, etc., for their excellent photocatalytic efficiency under UV light and energy band gap (Figure 9), but an important parameter to consider is photocatalyst deactivation [171].

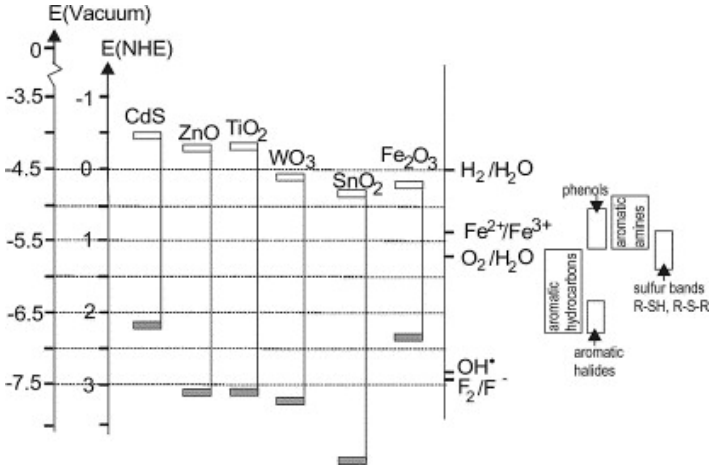

Figure 9. Band positions (top of valence band and bottom of conduction band) of several semiconductors together with some selected redox potentials. Reprinted from [172]. Copyright (2004), with permission from Elsevier.

This phenomenon depends on the reaction ambient; indeed, during the photocatalytic reaction, the photocatalyst will be constantly exposed to light and mixtures of fresh and treated solutions containing a variety of pollutants (target and non-target). In this way, the accumulation of various organics, including the parental organics, intermediates, and non-target pollutants, will likely occur (via adsorption) on the surface of the photocatalyst. This is a problem because it causes a dramatic decrease in photocatalytic activity (degradation of organics) [173,174]. Liqiang et al. [175] examined the lifetimes of ZnO and TiO_2 nanoparticles in the gas-phase photocatalytic oxidation of n-C_7H_{16} or SO_2. The obtained results showed that ZnO could be deactivated in the gas-phase photocatalytic oxidation of n-C_7H_{16}, while TiO_2 could nearly retain its activity. In the gas-phase photocatalytic oxidation of SO_2, ZnO, and TiO_2 could both be deactivated. They justified the deactivation after photocatalytic reaction via the adsorption of the oxidation products such as H_2O, CO_2, and SO_3 on the semiconductor photocatalyst surface. For these reasons, generally, after some cycles of reaction, the regeneration of the photocatalyst is necessary. In a review by Yan Tang et al. [176], various aspects such as lifetime, deactivation mechanism, and regeneration efficiency/characterization of deactivated photocatalysts were discussed. The deactivation of the photocatalyst in the photocatalytic degradation of methyl orange (MO) was studied by Yan Li et al. [177], who observed that it was not due to pore blocking by the reactant (MO) or intermediate products but due to the surface adsorption of MO and reaction intermediates. The spent photocatalysts were regenerated after washing with methanol and hydrogen peroxide (H_2O_2) and then treated with heat. H_2O_2 treatment generated the highest regeneration rate because H_2O_2 is a strong oxidizing agent that oxidized the deposited species on the surface of the photocatalyst. In other studies, regeneration was accomplished with different methods such as the use of basifying agents [178], thermal process [179], use of UV irradiation, and oxidation with H_2O_2 [180,181].

The problem of photocatalyst deactivation described in this section allows us to anticipate the easy maintenance of PMR plants because, among other components, photocatalysts may also need a regeneration program.

4. Analysis of the Main PMR Configurations Related to the Main Parameters of a Tertiary Stage

As described in the previous sections, the basic configurations of PMRs are the photocatalytic membranes (using organic or inorganic membranes), where the photocatalyst is immobilized in/on the membrane, which is used as support, and the slurry–PMRs, where the photocatalyst is suspended in the reaction media, and the membrane is able to confine the photocatalyst in the photoreaction zone. In these two configurations, numerous

sub-configurations have been proposed, and some of them have been described before. However, here, a gross comparison between these two basic configurations is provided to identify which one seems more suitable for a tertiary sewage WWT. The fact that sewage WWTPs operate continuously requires maintaining optimal conditions constantly. This means that solar light (available only during the day) for direct photocatalyst irradiation must be excluded, but it can be considered as a photovoltaic electrical energy source (e.g., accumulation system) for the integration of the electrical energy required to power the lamps. Furthermore, it is known that the intensity of solar radiation is variable during the day, so a variable photodegradation rate will be obtained during the day. The composition of wastewater from the secondary stage could be variable during this time, so a slurry–PMR will mitigate these oscillations better than a photocatalytic membrane, resulting in less oscillation of the photodegradation rate. The quality of the water from the tertiary stage could be controlled with various types of membranes (NF or RO), mainly the spiral-wound type widely used in many large-scale plants. The plant footprint is strongly dependent on the type of photocatalyst confinement. The immobilized photocatalyst is present as a layer to maximize the exposed surface to the light, but this also gives a high plant footprint compared with a slurry–PMR, where the same photocatalyst amount is suspended in a CSTR photoreactor with a smaller footprint (see Section 3.5). Furthermore, the irradiation of the photocatalytic layer requires (in continuous operation) external frontal lamps. Instead, cylindrical bulb lamps, immersed in the slurry, can irradiate at 360° with increased efficiency of the required electrical energy. With the use of external lamps, the photocatalytic layer in/on the photocatalytic membrane can also be placed in vertical mode to reduce the plant footprint. However, a drawback of this configuration still exists. Indeed, all immobilized photocatalyst particles are always illuminated on the same side and can be subject to a shorter life cycle than a slurry–CSTR. If we consider a photocatalyst particle having a spherical shape, this particle could be covered in some part of the surface by adsorbed species that inactivate that part to photonic excitation. If particles are suspended, they can move and rotate in all directions and can be subject to excitation on the other parts of the spherical surface. Indeed, the loss of active photocatalyst surface for the immobilized photocatalysts is higher than for suspended photocatalysts (the initial available active surface is that of all spherical surfaces for suspended particles, while it is a spherical cup for immobilized particles). This last aspect requires a more frequent regeneration in the case of immobilized photocatalysts. The regeneration in the case of slurry–CSTR systems is conceptually simple: the cessation of aeration allows for the sedimentation of particles that can be removed and substituted by a fresh photocatalyst. In the case of immobilized photocatalysts, depending on the type of immobilization, this operation can be quite difficult and could require the substitution of the overall photocatalytic membrane with a significant increase in maintenance costs. The final assessment of the six parameters discussed in Section 3 is reported in Table 2, which provides a quick overview of which configuration of PMR could be more suitable in a tertiary sewage WWT. It should be noted that all the described features have been considered for a specific type of wastewater, but for other types of wastewater, other specific parameters should be found and analyzed.

Table 2. Suitability or unsuitability of each of the six parameters to fit the requirement of a tertiary stage of wastewater treatment for the main configurations of PMRs.

Configuration of PMR	Continuous Wastewater Flow Rate (Section 3.1)	Self-Control of the Photodegradation Rate (Section 3.2)	Ability to Handle Variations of Concentrations and Flow Rate (Section 3.3)	Control of the Quality of the Treated Wastewater (Section 3.4)	Low Footprint (Section 3.5)	Easy Maintenance (Section 3.6)
Photocatalytic membrane	Yes	No	No	No	No	No
Slurry–CSTR PMR	Yes	Yes	Yes	Yes	Yes	Yes

As shown in Table 2, the slurry–CSTR PMR seems the most suitable configuration. In particular, the configuration employing a gravity filter to keep the photocatalyst in the reaction in the reaction zone and an NF or RO membrane to control the residence time of pollutants in the photoreactor seems, at this stage of knowledge, the specific configuration on that the research efforts should be concentrated. Furthermore, as widely described in the review of Rueda-Marquez et al. [182], extensive studies on real wastewater detoxification using photocatalysts are also needed.

The conclusion reached in this analysis (slurry/suspended photocatalysts perform better than immobilized photocatalysts) is focused on the comparison between the two basic PMR configurations in a particular application (tertiary sewage treatment), considering the possibility of obtaining volumes of good quality water available for reuse. However, other than this first type of comparison, to decide if slurry–PMR systems are advantageous or not at an industrial scale, a comparison with other technologies in tertiary wastewater treatment, by means of sustainability assessment, including the associated economics, must also be carried out.

Multi-criteria analysis was carried out by Plakas et al. [183] to assess four tertiary wastewater treatment (WWT) technologies regarding their sustainability performance to obtain useful information for designers and decision makers. The technologies were powdered activated carbon adsorption coupled with ultrafiltration membrane separation (PAC-UF), reverse osmosis, ozone/ultraviolet-light oxidation, and heterogeneous photocatalysis coupled with low-pressure membrane separation (PMR). Although the PAC-UF technology appeared to be the most appropriate, PMR was highlighted as the technology configuration. In particular, the configuration employing a gravity filter to keep the photocatalyst in the reaction under ambient conditions and an NF or RO membrane to control the residence with the least variability in its performance. For carrying out an assessment for the comparison of similar water treatment processes, it is necessary to use appropriate performance indicators to take into account economic issues like equipment capital expenses, operating expenses, and sustainability assessment, considering the fact that, for specific applications, the selection of the appropriate water treatment technology should be made on the basis of "triple bottom line" (TBL), i.e., by using environmental, economic and social criteria [184].

Concerning the cost estimation of a PMR, Samhaber and Nguyen [185] evaluated the costs separately because of the specific different nature of the photocatalytic part and the membrane part. The cost items are energy, membrane, chemicals, capital, UV–visible lamp replacement, personnel, etc., which are converted into unit cost per m^3 of treated water. The cost estimation [185] among various AOPs like H_2O_2/medium-pressure UV, H_2O_2/O_3, hydrodynamic cavitation with H_2O_2, and TiO_2 photocatalysis under UV (without membrane) showed that, for the first three technologies, the costs were in the range of 0.71–1.13 USD/1000 gallons treated (0.19–0.30 USD/m^3) for a TOC in the range 0–8–8 mg/L, while for photocatalysis–UV, they increased from 1.68 USD/1000 gallons to 3.08 USD/1000 gallons (0.44–0.81 USD/m^3) with the increase in TOC. This happens because the treatment

of higher TOC concentration effluent will surely lead to a shorter photocatalyst lifetime and more often reactor and lamp cleaning. Another cost estimation was carried out by Rani and Karthikeyan [186] on the degradation of a mixture of polycyclic aromatic hydrocarbons (PAHs) in a UV slurry photocatalytic membrane reactor. They compared photocatalysis (UV-TiO_2), membrane separation (MS), and integrated photocatalytic membrane (UV-TiO_2 + MS) and found that UV-TiO_2 + MS could be successful based upon the operating time and operational costs, as the operating time was twice lesser than the conventional UV-TiO_2 process. They estimated a treatment cost per m^3 of effluent containing PAHs in PMR to be USD 10.4 to USD 3.6.

The results of cost estimation are generally expressed as cost/m^3, but an important aspect to be considered is the source of the used data. They can come from a laboratory plant or plants of different sizes, but the same scale factor (e.g., same treated water flow rates) should be considered when different technologies are compared. Indeed, for the same technology, it is also well known that the costs/m^3 for plants of larger sizes are generally lower than that of smaller sizes. These factors should also be considered in research, and this means that more data are needed on pilot plants of suitable size for PMRs to obtain reliable information for decision makers.

5. Conclusions

The research on photocatalytic membrane reactors (PMRs) has shown their great potential in wastewater treatment, and some studies are at bench scale and pilot plant level. The field of sewage wastewater treatment involves very high flow rates, so high volumes of good-quality treated water could be reused for various purposes provided an efficient tertiary treatment is available. PMRs could mineralize many recalcitrant pollutants in the tertiary stage to reach the requested quality also due to the use of selective NF or RO membranes. The analysis of the two main configurations of PMRs (photocatalytic membranes and slurry–PMRs) was carried out using six design and operational parameters, concerning the sewage wastewater treatment: (i) a continuous wastewater flow rate from the secondary stage; (ii) the self-control of the photodegradation rate related to wastewater chemical–physical parameters; (iii) the ability to handle variations in concentration and wastewater flow rate; (iv) the control of the quality of treated wastewater; (v) low plant footprint; and (vi) easy maintenance. Important findings that emerged are the continuous flow of real industrial effluents and the very high flow rates that prompt, as future research, the use of PMR configurations with continuous illumination (e.g., low-energy-consuming LED lamps), a photodegradation rate with small oscillation, membranes with high packing density able to work at high flux and high rejection rates versus recalcitrant pollutants, low footprint design, and the easy substitution of the photocatalyst when it is deactivated. All these points seem fit well, at the current state of knowledge, with the choice of slurry–PMRs compared with photocatalytic membranes. Furthermore, research on mixtures of different photocatalysts is needed to optimize the photodegradation rate on a wide range of pollutants as well as the use of real wastewater (or mixtures of various pollutants) to obtain information on the robustness of PMR technology. Tests on pilot PMR plants of suitable size are required to obtain reliable data for performing a sustainability assessment of the slurry–PMR process compared with other processes already used in tertiary wastewater treatment. With this study, it is envisioned that researchers could acquire a good direction for the development of future research in the effort to bring photocatalysis combined with membranes to practical application in the reuse of sewage wastewater.

Author Contributions: R.M.: conceptualization, literature overview, writing—original draft preparation, supervision. A.S.: literature overview, writing—original draft preparation, writing—review and editing. C.L.: literature overview, writing—original draft preparation, writing—review and editing. P.A.: literature overview, writing—original draft preparation, writing—review and editing. All authors have read and agreed to the published version of the manuscript.

Funding: This research was funded by the project "Tech4You—Technologies for climate change adaptation and quality of life improvement"—National Recovery and Resilience Plan (NRRP), Mission 4, Component 2, Investment 1.5, funded from the European Union–NextGenerationEU, identity code: ECS 00000009, CUP H23C22000370006.

Data Availability Statement: Not applicable.

Acknowledgments: The autors thank the project "Tech4You—Technologies for climate change adaptation and quality of life improvement"—National Recovery and Resilience Plan (NRRP), Mission 4, Component 2, Investment 1.5, funded from the European Union–NextGenerationEU, identity code: ECS 00000009, CUP H23C22000370006. C. Lavorato thanks Regione Calabria in POR Calabria FESR FSE 2014-2020 for the RTDa financial support.

Conflicts of Interest: The authors declare that they have no known competing financial interests or personal relationships that could have appeared to influence the work reported in this paper.

References

1. Deng, S.; Hu, J.; Ong, S.-L.; Li, Q.; Han, J. Advanced technologies for industrial wastewater reclamation. *Front. Environ. Sci.* **2023**, *11*, 542. [CrossRef]
2. Toray Membrane USA. Optimizing RO-Membrane Performance in Produced-Water Applications. Available online: https://www.wateronline.com/doc/optimizing-ro-membrane-performance-in-produced-water-applications-0001?vm_tId=2518845&vm_nId=80299&user=0038f1ed-66e0-46bd-91e2-ebaf82420db6&gdpr=1&vm_alias=O (accessed on 14 July 2023).
3. Cacace, D.; Fatta-Kassinos, D.; Manaia, C.M.; Cytryn, E.; Kreuzinger, N.; Rizzo, L.; Karaolia, P.; Schwartz, T.; Alexander, J.; Merlin, C.; et al. Antibiotic resistance genes in treated wastewater and in the receiving water bodies: A pan-European survey of urban settings. *Water Res.* **2019**, *162*, 320–330. [CrossRef] [PubMed]
4. Corno, G.; Yang, Y.; Eckert, E.M.; Fontaneto, D.; Fiorentino, A.; Galafassi, S.; Zhang, T.; Di Cesare, A. Effluents of wastewater treatment plants promote the rapid stabilization of the antibiotic resistome in receiving freshwater bodies. *Water Res.* **2019**, *158*, 72–81. [CrossRef] [PubMed]
5. Manaia, C.M.; Rocha, J.; Scaccia, N.; Marano, R.; Radu, E.; Biancullo, F.; Cerqueira, F.; Fortunato, G.; Iakovides, I.C.; Zammit, I.; et al. Antibiotic resistance in wastewater treatment plants: Tackling the black box. *Environ. Int.* **2018**, *115*, 312–324. [CrossRef]
6. Osińska, A.; Korzeniewska, E.; Harnisz, M.; Felis, E.; Bajkacz, S.; Jachimowicz, P.; Niestępski, S.; Konopka, I. Small-scale wastewater treatment plants as a source of the dissemination of antibiotic resistance genes in the aquatic environment. *J. Hazard. Mater.* **2020**, *381*, 121221. [CrossRef] [PubMed]
7. Farré, M.l.; Pérez, S.; Kantiani, L.; Barceló, D. Fate and toxicity of emerging pollutants, their metabolites and transformation products in the aquatic environment. *TrAC Trends Anal. Chem.* **2008**, *27*, 991–1007. [CrossRef]
8. García, J.; García-Galán, M.J.; Day, J.W.; Boopathy, R.; White, J.R.; Wallace, S.; Hunter, R.G. A review of emerging organic contaminants (EOCs), antibiotic resistant bacteria (ARB), and antibiotic resistance genes (ARGs) in the environment: Increasing removal with wetlands and reducing environmental impacts. *Bioresour. Technol.* **2020**, *307*, 123228. [CrossRef]
9. Niu, L.; Liu, W.; Juhasz, A.; Chen, J.; Ma, L. Emerging contaminants antibiotic resistance genes and microplastics in the environment: Introduction to 21 review articles published in CREST during 2018–2022. *Crit. Rev. Environ. Sci. Technol.* **2022**, *52*, 4135–4146. [CrossRef]
10. Sharma, A.; Pandit, P.; Chopade, R.; Nagar, V.; Aseri, V.; Singh, A.; Awasthi, K.; Awasthi, G.; Singh Sankhla, M. Eradication of Microplastics in Wastewater Treatment: Overview. *Biointerface Res. Appl. Chem.* **2022**, *13*, 223. [CrossRef]
11. Liu, F.; Guan, X.; Xiao, F. Photodegradation of per- and polyfluoroalkyl substances in water: A review of fundamentals and applications. *J. Hazard. Mater.* **2022**, *439*, 129580. [CrossRef]
12. Harmsco Filtration Products. Understanding Options Key to Selecting Most Effective, Lowest Cost PFAS Solution. Available online: https://www.wateronline.com/doc/understanding-options-key-to-selecting-most-effective-lowest-cost-pfas-solution-0001?vm_tId=2523322&vm_nId=80411&user=0038f1ed-66e0-46bd-91e2-ebaf82420db6&gdpr=1&vm (accessed on 14 July 2023).
13. Koyuncuoğlu, P.; Erden, G. Microplastics in municipal wastewater treatment plants: A case study of Denizli/Turkey. *Front. Environ. Sci. Eng.* **2023**, *17*, 99. [CrossRef]
14. Vazquez, L.; Gomes, L.M.M.T.; Presumido, P.H.; Rocca, D.G.D.; Moreira, R.F.P.M.; Dagnac, T.; Llompart, M.; Gomes, A.I.; Vilar, V.J.P. Tubular membrane photoreactor for the tertiary treatment of urban wastewater towards antibiotics removal: Application of different photocatalyst/oxidant combinations and ozonation. *J. Environ. Chem. Eng.* **2023**, *11*, 109766. [CrossRef]
15. Jippe Hoogeveen (FAO). Monitoring Water Use in Agriculture through Satellite Remote Sensing, Future of Water. 2021. Available online: https://www.globalcause.co.uk/water/monitoring-water-use-in-agriculture-through-satellite-remote-sensing/#utm_source=FAO-distro&utm_medium=client (accessed on 4 August 2023).
16. Mangla, D.; Annu; Sharma, A.; Ikram, S. Critical review on adsorptive removal of antibiotics: Present situation, challenges and future perspective. *J. Hazard. Mater.* **2022**, *425*, 127946. [CrossRef] [PubMed]

17. Rizzo, L.; Malato, S.; Antakyali, D.; Beretsou, V.G.; Đolić, M.B.; Gernjak, W.; Heath, E.; Ivancev-Tumbas, I.; Karaolia, P.; Lado Ribeiro, A.R.; et al. Consolidated vs new advanced treatment methods for the removal of contaminants of emerging concern from urban wastewater. *Sci. Total Environ.* **2019**, *655*, 986–1008. [CrossRef]
18. Cuerda-Correa, E.M.; Alexandre-Franco, M.F.; Fernández-González, C. Advanced Oxidation Processes for the Removal of Antibiotics from Water. An Overview. *Water* **2020**, *12*, 102. [CrossRef]
19. Lama, G.; Meijide, J.; Sanromán, A.; Pazos, M. Heterogeneous Advanced Oxidation Processes: Current Approaches for Wastewater Treatment. *Catalysts* **2022**, *12*, 344. [CrossRef]
20. Ahmad, I.; Zou, Y.; Yan, J.; Liu, Y.; Shukrullah, S.; Naz, M.Y.; Hussain, H.; Khan, W.Q.; Khalid, N.R. Semiconductor photocatalysts: A critical review highlighting the various strategies to boost the photocatalytic performances for diverse applications. *Adv. Colloid Interface Sci.* **2023**, *311*, 102830. [CrossRef]
21. Binjhade, R.; Mondal, R.; Mondal, S. Continuous photocatalytic reactor: Critical review on the design and performance. *J. Environ. Chem. Eng.* **2022**, *10*, 107746. [CrossRef]
22. Vaiano, V.; Sacco, O.; Pisano, D.; Sannino, D.; Ciambelli, P. From the design to the development of a continuous fixed bed photoreactor for photocatalytic degradation of organic pollutants in wastewater. *Chem. Eng. Sci.* **2015**, *137*, 152–160. [CrossRef]
23. Sopyan, I.; Watanabe, M.; Murasawa, S.; Hashimoto, K.; Fujishima, A. A film-type photocatalyst incorporating highly active TiO_2 powder and fluororesin binder: Photocatalytic activity and long-term stability. *J. Electroanal. Chem.* **1996**, *415*, 183–186. [CrossRef]
24. Molinari, R.; Lavorato, C.; Argurio, P. The Evolution of Photocatalytic Membrane Reactors over the Last 20 Years: A State of the Art Perspective. *Catalysts* **2021**, *11*, 775. [CrossRef]
25. Mozia, S. Photocatalytic membrane reactors (PMRs) in water and wastewater treatment. A review. *Sep. Purif. Technol.* **2010**, *73*, 71–91. [CrossRef]
26. Kundu, S.; Karak, N. Polymeric photocatalytic membrane: An emerging solution for environmental remediation. *Chem. Eng. J.* **2022**, *438*, 135575. [CrossRef]
27. Zagklis, D.P.; Bampos, G. Tertiary Wastewater Treatment Technologies: A Review of Technical, Economic, and Life Cycle Aspects. *Processes* **2022**, *10*, 2304. [CrossRef]
28. Zagklis, D.; Katrivesis, F.K.; Sygouni, V.; Tsarouchi, L.; Tsigkou, K.; Kornaros, M.; Paraskeva, C.A. Recovery of Water from Secondary Effluent through Pilot Scale Ultrafiltration Membranes: Implementation at Patras' Wastewater Treatment Plant. *Membranes* **2021**, *11*, 663. [CrossRef] [PubMed]
29. Ganiyu, S.O.; Van Hullebusch, E.D.; Cretin, M.; Esposito, G.; Oturan, M.A. Coupling of membrane filtration and advanced oxidation processes for removal of pharmaceutical residues: A critical review. *Sep. Purif. Technol.* **2015**, *156*, 891–914. [CrossRef]
30. Espíndola, J.C.; Cristóvão, R.O.; Mendes, A.; Boaventura, R.A.R.; Vilar, V.J.P. Photocatalytic membrane reactor performance towards oxytetracycline removal from synthetic and real matrices: Suspended vs immobilized TiO_2-P25. *Chem. Eng. J.* **2019**, *378*, 122114. [CrossRef]
31. Chakraborty, S.; Loutatidou, S.; Palmisano, G.; Kujawa, J.; Mavukkandy, M.O.; Al-Gharabli, S.; Curcio, E.; Arafat, H.A. Photocatalytic hollow fiber membranes for the degradation of pharmaceutical compounds in wastewater. *J. Environ. Chem. Eng.* **2017**, *5*, 5014–5024. [CrossRef]
32. Molinari, R.; Lavorato, C.; Argurio, P. Application of Hybrid Membrane Processes Coupling Separation and Biological or Chemical Reaction in Advanced Wastewater Treatment. *Membranes* **2020**, *10*, 281. [CrossRef]
33. Ramos, B.; Parisi Couri, A.; Ookawara, S.; Silva Costa Teixeira, A.C. Micro-structured packed bed reactors for solar photocatalysis: Impacts of packing size and material on light harnessing. *Photochem. Photobiol. Sci.* **2019**, *18*, 577–582. [CrossRef]
34. Bales, C.; Lian, B.; Zhu, Y.; Zhou, H.; Wang, Y.; Fletcher, J.; Waite, T.D. Photovoltaic powered operational scale Membrane Capacitive Deionization (MCDI) desalination with energy recovery for treated domestic wastewater reuse. *Desalination* **2023**, *559*, 116647. [CrossRef]
35. Augugliaro, V.; García-López, E.; Loddo, V.; Malato-Rodríguez, S.; Maldonado, I.; Marcì, G.; Molinari, R.; Palmisano, L. Degradation of lincomycin in aqueous medium: Coupling of solar photocatalysis and membrane separation. *Sol. Energy* **2005**, *79*, 402–408. [CrossRef]
36. Hart, O.E.; Halden, R.U. Modeling wastewater temperature and attenuation of sewage-borne biomarkers globally. *Water Res.* **2020**, *172*, 115473. [CrossRef] [PubMed]
37. Loddo, V.; Bellardita, M.; Camera-Roda, G.; Parrino, F.; Palmisano, L. Chapter 1—Heterogeneous Photocatalysis: A Promising Advanced Oxidation Process. In *Current Trends and Future Developments on (Bio-) Membranes*; Basile, A., Mozia, S., Molinari, R., Eds.; Elsevier: Amsterdam, The Netherlands, 2018; pp. 1–43.
38. Tang, W.Z.; Huren, A. UV/TiO_2 photocatalytic oxidation of commercial dyes in aqueous solutions. *Chemosphere* **1995**, *31*, 4157–4170. [CrossRef]
39. Ge, J.; Zhang, Z.; Ouyang, Z.; Shang, M.; Liu, P.; Li, H.; Guo, X. Photocatalytic degradation of (micro)plastics using TiO_2-based and other catalysts: Properties, influencing factor, and mechanism. *Environ. Res.* **2022**, *209*, 112729. [CrossRef]
40. Chen, J.; He, Z.; Ji, Y.; Li, G.; An, T.; Choi, W. OH radicals determined photocatalytic degradation mechanisms of gaseous styrene in TiO_2 system under 254 nm versus 185 nm irradiation: Combined experimental and theoretical studies. *Appl. Catal. B Environ.* **2019**, *257*, 117912. [CrossRef]

41. Chen, J.; Zhang, Z.; Zhu, W.; Zhang, L.; Zhao, B.; Ji, Y.; Li, G.; An, T. Superoxide radical enhanced photocatalytic performance of styrene alters its degradation mechanism and intermediate health risk on TiO_2/graphene surface. *Environ. Res.* **2021**, *195*, 110747. [CrossRef]
42. Xu, M.; Chen, Y.; Qin, J.; Feng, Y.; Li, W.; Chen, W.; Zhu, J.; Li, H.; Bian, Z. Unveiling the Role of Defects on Oxygen Activation and Photodegradation of Organic Pollutants. *Environ. Sci. Technol.* **2018**, *52*, 13879–13886. [CrossRef]
43. Li, Z.; Luan, Y.; Qu, Y.; Jing, L. Modification Strategies with Inorganic Acids for Efficient Photocatalysts by Promoting the Adsorption of O_2. *ACS Appl. Mater. Interfaces* **2015**, *7*, 22727–22740. [CrossRef]
44. Hoffmann, M.R.; Martin, S.T.; Choi, W.; Bahnemann, D.W. Environmental Applications of Semiconductor Photocatalysis. *Chem. Rev.* **1995**, *95*, 69–96. [CrossRef]
45. Braun, A.M.; Oliveros, E. How to evaluate photochemical methods for water treatment. *Water Sci. Technol.* **1997**, *35*, 17–23. [CrossRef]
46. Zhang, X.; Li, X.; Yu, P.; Yu, Y.; Fan, X.; Zhang, J.; Yu, Y.; Zheng, H.; Sun, Y. Photocatalytic O_2 activation by metal-free carbon nitride nanotube for rapid reactive species generation and organic contaminants degradation. *J. Hazard. Mater.* **2023**, *456*, 131715. [CrossRef]
47. Ma, H.-Y.; Zhao, L.; Guo, L.-H.; Zhang, H.; Chen, F.-J.; Yu, W.-C. Roles of reactive oxygen species (ROS) in the photocatalytic degradation of pentachlorophenol and its main toxic intermediates by TiO_2/UV. *J. Hazard. Mater.* **2019**, *369*, 719–726. [CrossRef] [PubMed]
48. Beranek, R. (Photo)electrochemical Methods for the Determination of the Band Edge Positions of TiO_2-Based Nanomaterials. *Adv. Phys. Chem.* **2011**, *2011*, 786759. [CrossRef]
49. Jacobsen, A.E. Titanium Dioxide Pigments: Correlation between Photochemical Reactivity and Chalking. *Ind. Eng. Chem.* **1949**, *41*, 523–526. [CrossRef]
50. Allé, P.H.; Garcia-Muñoz, P.; Adouby, K.; Keller, N.; Robert, D. Efficient photocatalytic mineralization of polymethylmethacrylate and polystyrene nanoplastics by TiO_2/β-SiC alveolar foams. *Environ. Chem. Lett.* **2021**, *19*, 1803–1808. [CrossRef]
51. Tan, S.Y.; Chong, W.C.; Sethupathi, S.; Pang, Y.L.; Sim, L.C.; Mahmoudi, E. Optimisation of aqueous phase low density polyethylene degradation by graphene oxide-zinc oxide photocatalysts. *Chem. Eng. Res. Des.* **2023**, *190*, 550–565. [CrossRef]
52. Viet, N.M.; Mai Huong, N.T.; Thu Hoai, P.T. Enhanced photocatalytic decomposition of phenol in wastewater by using La–TiO_2 nanocomposite. *Chemosphere* **2023**, *313*, 137605. [CrossRef] [PubMed]
53. Ur Rahman, Z.; Shah, U.; Alam, A.; Shah, Z.; Shaheen, K.; Bahadar Khan, S.; Ali Khan, S. Photocatalytic degradation of cefixime using CuO-NiO nanocomposite photocatalyst. *Inorg. Chem. Commun.* **2023**, *148*, 110312. [CrossRef]
54. Doong, R.-A.; Chen, C.-H.; Maithreepala, R.A.; Chang, S.-M. The influence of pH and cadmium sulfide on the photocatalytic degradation of 2-chlorophenol in titanium dioxide suspensions. *Water Res.* **2001**, *35*, 2873–2880. [CrossRef]
55. Mirzaei, A.; Yerushalmi, L.; Chen, Z.; Haghighat, F.; Guo, J. Enhanced photocatalytic degradation of sulfamethoxazole by zinc oxide photocatalyst in the presence of fluoride ions: Optimization of parameters and toxicological evaluation. *Water Res.* **2018**, *132*, 241–251. [CrossRef] [PubMed]
56. Liu, S.; Yu, J.; Cheng, B.; Jaroniec, M. Fluorinated semiconductor photocatalysts: Tunable synthesis and unique properties. *Adv. Colloid Interface Sci.* **2012**, *173*, 35–53. [CrossRef]
57. Park, H.; Choi, W. Effects of TiO_2 Surface Fluorination on Photocatalytic Reactions and Photoelectrochemical Behaviors. *J. Phys. Chem. B* **2004**, *108*, 4086–4093. [CrossRef]
58. Herrmann, J.M. Heterogeneous photocatalysis: State of the art and present applications. *Top. Catal.* **2005**, *34*, 49–65. [CrossRef]
59. Matthews, R.W. Hydroxylation reactions induced by near-ultraviolet photolysis of aqueous titanium dioxide suspensions. *J. Chem. Soc. Faraday Trans. 1 Phys. Chem. Condens. Phases* **1984**, *80*, 457–471. [CrossRef]
60. Ariza-Tarazona, M.C.; Villarreal-Chiu, J.F.; Hernández-López, J.M.; Rivera De la Rosa, J.; Barbieri, V.; Siligardi, C.; Cedillo-González, E.I. Microplastic pollution reduction by a carbon and nitrogen-doped TiO_2: Effect of pH and temperature in the photocatalytic degradation process. *J. Hazard. Mater.* **2020**, *395*, 122632. [CrossRef]
61. Liu, L.; Xu, M.; Ye, Y.; Zhang, B. On the degradation of (micro)plastics: Degradation methods, influencing factors, environmental impacts. *Sci. Total Environ.* **2022**, *806*, 151312. [CrossRef]
62. Gao, D.; Yang, H.; Shu, Z. The preparation of Ag@AgCl photocatalytic material based on the photocatalysis material CA+ and degradation of tetracycline. *J. Exp. Nanosci.* **2023**, *18*, 2162509. [CrossRef]
63. Maqbool, S.; Ahmed, A.; Mukhtar, A.; Jamshaid, M.; Rehman, A.U.; Anjum, S. Efficient photocatalytic degradation of Rhodamine B dye using solar light-driven La-Mn co-doped Fe_2O_3 nanoparticles. *Environ. Sci. Pollut. Res.* **2023**, *30*, 7121–7137. [CrossRef]
64. Ishaque, F.; Ahn, Y.-H. Critical parameters influencing the continuous performance of upflow microbubble airlift photocatalytic process treating pharmaceutical pollutants. *Chemosphere* **2023**, *332*, 138887. [CrossRef]
65. Khan, A.A.; Tahir, M. Recent advancements in engineering approach towards design of photo-reactors for selective photocatalytic CO_2 reduction to renewable fuels. *J. CO_2 Util.* **2019**, *29*, 205–239. [CrossRef]
66. Barquín, C.; Vital-Grappin, A.; Kumakiri, I.; Diban, N.; Rivero, M.J.; Urtiaga, A.; Ortiz, I. Performance of TiO_2-Based Tubular Membranes in the Photocatalytic Degradation of Organic Compounds. *Membranes* **2023**, *13*, 448. [CrossRef] [PubMed]
67. Bansal, P.; Verma, A. Pilot-scale single-step reactor combining photocatalysis and photo-Fenton aiming at faster removal of Cephalexin. *J. Clean. Prod.* **2018**, *195*, 540–551. [CrossRef]

68. Tokode, O.; Prabhu, R.; Lawton, L.A.; Robertson, P.K.J. Controlled periodic illumination in semiconductor photocatalysis. *J. Photochem. Photobiol. A Chem.* **2016**, *319–320*, 96–106. [CrossRef]
69. Jo, W.K.; Park, G.T.; Tayade, R.J. Synergetic effect of adsorption on degradation of malachite green dye under blue LED irradiation using spiral-shaped photocatalytic reactor. *J. Chem. Technol. Biotechnol.* **2015**, *90*, 2280–2289. [CrossRef]
70. Ray, A.K. Photocatalytic Reactor Configurations for Water Purification: Experimentation and Modeling. In *Advances in Chemical Engineering*; de Lasa, H.I., Serrano Rosales, B., Eds.; Academic Press: Cambridge, MA, USA, 2009; Volume 36, pp. 145–184.
71. Sacco, O.; Vaiano, V.; Sannino, D. Main parameters influencing the design of photocatalytic reactors for wastewater treatment: A mini review. *J. Chem. Technol. Biotechnol.* **2020**, *95*, 2608–2618. [CrossRef]
72. Kowalska, E.; Rau, S. Photoreactors for wastewater treatment: A review. *Recent Pat. Eng.* **2010**, *4*, 242–266. [CrossRef]
73. Lavorato, C.; Argurio, P.; Mastropietro, T.F.; Pirri, G.; Poerio, T.; Molinari, R. Pd/TiO_2 doped faujasite photocatalysts for acetophenone transfer hydrogenation in a photocatalytic membrane reactor. *J. Catal.* **2017**, *353*, 152–161. [CrossRef]
74. Molinari, R.; Lavorato, C.; Argurio, P. Photocatalytic reduction of acetophenone in membrane reactors under UV and visible light using TiO_2 and Pd/TiO_2 catalysts. *Chem. Eng. J.* **2015**, *274*, 307–316. [CrossRef]
75. Molinari, R.; Limonti, C.; Lavorato, C.; Siciliano, A.; Argurio, P. Upgrade of a slurry photocatalytic membrane reactor based on a vertical filter and an external membrane and testing in the photodegradation of a model pollutant in water. *Chem. Eng. J.* **2023**, *451*, 138577. [CrossRef]
76. Molinari, R.; Lavorato, C.; Argurio, P. Visible-Light Photocatalysts and Their Perspectives for Building Photocatalytic Membrane Reactors for Various Liquid Phase Chemical Conversions. *Catalysts* **2020**, *10*, 1334. [CrossRef]
77. Salaices, M.; Serrano, B.; de Lasa, H.I. Experimental evaluation of photon absorption in an aqueous TiO_2 slurry reactor. *Chem. Eng. J.* **2002**, *90*, 219–229. [CrossRef]
78. Rani, C.N.; Karthikeyan, S. Performance of an indigenous integrated slurry photocatalytic membrane reactor (PMR) on the removal of aqueous phenanthrene (PHE). *Water Sci. Technol.* **2018**, *77*, 2642–2656. [CrossRef]
79. Mukherjee, P.S.; Ray, A.K. Major challenges in the design of a large-scale photocatalytic reactor for water treatment. *Chem. Eng. Technol.* **1999**, *22*, 253–260. [CrossRef]
80. Wang, D.; Mueses, M.A.; Márquez, J.A.C.; Machuca-Martínez, F.; Grčić, I.; Peralta Muniz Moreira, R.; Li Puma, G. Engineering and modeling perspectives on photocatalytic reactors for water treatment. *Water Res.* **2021**, *202*, 117421. [CrossRef]
81. Casado, C.; Timmers, R.; Sergejevs, A.; Clarke, C.T.; Allsopp, D.W.E.; Bowen, C.R.; van Grieken, R.; Marugán, J. Design and validation of a LED-based high intensity photocatalytic reactor for quantifying activity measurements. *Chem. Eng. J.* **2017**, *327*, 1043–1055. [CrossRef]
82. O'Neal Tugaoen, H.; Garcia-Segura, S.; Hristovski, K.; Westerhoff, P. Compact light-emitting diode optical fiber immobilized TiO_2 reactor for photocatalytic water treatment. *Sci. Total Environ.* **2018**, *613–614*, 1331–1338. [CrossRef]
83. Ling, L.; Tugaoen, H.; Brame, J.; Sinha, S.; Li, C.; Schoepf, J.; Hristovski, K.; Kim, J.-H.; Shang, C.; Westerhoff, P. Coupling Light Emitting Diodes with Photocatalyst-Coated Optical Fibers Improves Quantum Yield of Pollutant Oxidation. *Environ. Sci. Technol.* **2017**, *51*, 13319–13326. [CrossRef]
84. Khademalrasool, M.; Farbod, M.; Talebzadeh, M.D. The improvement of photocatalytic processes: Design of a photoreactor using high-power LEDs. *J. Sci. Adv. Mater. Devices* **2016**, *1*, 382–387. [CrossRef]
85. Alpert, D.J.; Sprung, J.L.; Pacheco, J.E.; Prairie, M.R.; Reilly, H.E.; Milne, T.A.; Nimlos, M.R. Sandia National Laboratories' work in solar detoxification of hazardous wastes. *Sol. Energy Mater.* **1991**, *24*, 594–607. [CrossRef]
86. Braham, R.J.; Harris, A.T. Review of Major Design and Scale-up Considerations for Solar Photocatalytic Reactors. *Ind. Eng. Chem. Res.* **2009**, *48*, 8890–8905. [CrossRef]
87. Gernjak, W.; Maldonado, M.I.; Malato, S.; Cáceres, J.; Krutzler, T.; Glaser, A.; Bauer, R. Pilot-plant treatment of olive mill wastewater (OMW) by solar TiO_2 photocatalysis and solar photo-Fenton. *Sol. Energy* **2004**, *77*, 567–572. [CrossRef]
88. Malato Rodríguez, S.; Blanco Gálvez, J.; Maldonado Rubio, M.I.; Fernández Ibáñez, P.; Alarcón Padilla, D.; Collares Pereira, M.; Farinha Mendes, J.; Correia de Oliveira, J. Engineering of solar photocatalytic collectors. *Sol. Energy* **2004**, *77*, 513–524. [CrossRef]
89. Lu, M. *Photocatalysis and Water Purification: From Fundamentals to Recent Applications*; John Wiley & Sons: Hoboken, NJ, USA, 2013.
90. Colina-Márquez, J.; Machuca-Martínez, F.; Li Puma, G. Photocatalytic Mineralization of Commercial Herbicides in a Pilot-Scale Solar CPC Reactor: Photoreactor Modeling and Reaction Kinetics Constants Independent of Radiation Field. *Environ. Sci. Technol.* **2009**, *43*, 8953–8960. [CrossRef]
91. Blanco Galvez, J.; Fernandez-Ibanez, P.; Malato, S. Solar Photocatalytic Detoxification and Disinfection of Water: Recent Overview. *J. Sol. Energy Eng.* **2007**, *129*, 4–15. [CrossRef]
92. Dionysiou, D.D.; Suidan, M.T.; Baudin, I.; Laîné, J.-M. Oxidation of organic contaminants in a rotating disk photocatalytic reactor: Reaction kinetics in the liquid phase and the role of mass transfer based on the dimensionless Damköhler number. *Appl. Catal. B Environ.* **2002**, *38*, 1–16. [CrossRef]
93. Mehling, S.; Schnabel, T.; Londong, J. Photocatalytic ozonation in an immersion rotary body reactor for the removal of micro-pollutants from the effluent of wastewater treatment plants. *Water Sci Technol* **2022**, *85*, 535–548. [CrossRef]
94. Abdel-Maksoud, Y.; Imam, E.; Ramadan, A. TiO_2 Solar Photocatalytic Reactor Systems: Selection of Reactor Design for Scale-up and Commercialization—Analytical Review. *Catalysts* **2016**, *6*, 138. [CrossRef]
95. Li Puma, G.; Yue, P.L. A Novel Fountain Photocatalytic Reactor for Water Treatment and Purification: Modeling and Design. *Ind. Eng. Chem. Res.* **2001**, *40*, 5162–5169. [CrossRef]

96. Portela, R.; Suárez, S.; Tessinari, R.F.; Hernández-Alonso, M.D.; Canela, M.C.; Sánchez, B. Solar/lamp-irradiated tubular photoreactor for air treatment with transparent supported photocatalysts. *Appl. Catal. B Environ.* **2011**, *105*, 95–102. [CrossRef]
97. Puma, G.L.; Yue, P.L. Modelling and design of thin-film slurry photocatalytic reactors for water purification. *Chem. Eng. Sci.* **2003**, *58*, 2269–2281. [CrossRef]
98. Puma, G.L.; Brucato, A. Dimensionless analysis of slurry photocatalytic reactors using two-flux and six-flux radiation absorption–scattering models. *Catal. Today* **2007**, *122*, 78–90. [CrossRef]
99. Hirt, B.; Hansjosten, E.; Hensel, A.; Gräf, V.; Stahl, M. Improvement of an annular thin film UV-C reactor by fluid guiding elements. *Innov. Food Sci. Emerg. Technol.* **2022**, *77*, 102988. [CrossRef]
100. Wang, D.; Li, Y.; Li, G.; Wang, C.; Zhang, W.; Wang, Q. Modeling of quantitative effects of water components on the photocatalytic degradation of 17α-ethynylestradiol in a modified flat plate serpentine reactor. *J. Hazard. Mater.* **2013**, *254–255*, 64–71. [CrossRef]
101. Murcia Mesa, J.J.; Hernández Niño, J.S.; González, W.; Rojas, H.; Hidalgo, M.C.; Navío, J.A. Photocatalytic Treatment of Stained Wastewater Coming from Handicraft Factories. A Case Study at the Pilot Plant Level. *Water* **2021**, *13*, 2705. [CrossRef]
102. Sopajaree, K.; Qasim, S.A.; Basak, S.; Rajeshwar, K. An integrated flow reactor-membrane filtration system for heterogeneous photocatalysis. Part II: Experiments on the ultrafiltration unit and combined operation. *J. Appl. Electrochem.* **1999**, *29*, 1111–1118. [CrossRef]
103. Molinari, R.; Mungari, M.; Drioli, E.; Di Paola, A.; Loddo, V.; Palmisano, L.; Schiavello, M. Study on a photocatalytic membrane reactor for water purification. *Catal. Today* **2000**, *55*, 71–78. [CrossRef]
104. Mastropietro, T.F.; Meringolo, C.; Poerio, T.; Scarpelli, F.; Godbert, N.; Di Profio, G.; Fontananova, E. Multistimuli Activation of TiO_2/α-Alumina Membranes for Degradation of Methylene Blue. *Ind. Eng. Chem. Res.* **2017**, *56*, 11049–11057. [CrossRef]
105. Geissen, S.U.; Xi, W.; Weidemeyer, A.; Vogelpohl, A.; Bousselmi, L.; Ghrabi, A.; Ennabli, A. Comparison of suspended and fixed photocatalytic reactor systems. *Water Sci. Technol.* **2001**, *44*, 245–249. [CrossRef]
106. Molinari, R.; Palmisano, L.; Drioli, E.; Schiavello, M. Studies on various reactor configurations for coupling photocatalysis and membrane processes in water purification. *J. Membr. Sci.* **2002**, *206*, 399–415. [CrossRef]
107. Shi, Y.; Huang, J.; Zeng, G.; Cheng, W.; Hu, J.; Shi, L.; Yi, K. Evaluation of self-cleaning performance of the modified g-C3N4 and GO based PVDF membrane toward oil-in-water separation under visible-light. *Chemosphere* **2019**, *230*, 40–50. [CrossRef]
108. Moslehyani, A.; Ismail, A.F.; Othman, M.H.D.; Matsuura, T. Design and performance study of hybrid photocatalytic reactor-PVDF/MWCNT nanocomposite membrane system for treatment of petroleum refinery wastewater. *Desalination* **2015**, *363*, 99–111. [CrossRef]
109. Dzinun, H.; Othman, M.H.D.; Ismail, A.F.; Matsuura, T.; Puteh, M.H.; Rahman, M.A.; Jaafar, J. Stability study of extruded dual layer hollow fibre membranes in a long operation photocatalysis process. *Polym. Test.* **2018**, *68*, 53–60. [CrossRef]
110. Molinari, R.; Pirillo, F.; Falco, M.; Loddo, V.; Palmisano, L. Photocatalytic degradation of dyes by using a membrane reactor. *Chem. Eng. Process. Process Intensif.* **2004**, *43*, 1103–1114. [CrossRef]
111. Zhang, J.; Wang, L.; Zhang, G.; Wang, Z.; Xu, L.; Fan, Z. Influence of azo dye-TiO_2 interactions on the filtration performance in a hybrid photocatalysis/ultrafiltration process. *J. Colloid Interface Sci.* **2013**, *389*, 273–283. [CrossRef] [PubMed]
112. Zheng, X.; Shen, Z.P.; Shi, L.; Cheng, R.; Yuan, D.H. Photocatalytic membrane reactors (PMRs) in water treatment: Configurations and influencing factors. *Catalysts* **2017**, *7*, 224. [CrossRef]
113. Zheng, X.; Wang, Q.; Chen, L.; Wang, J.; Cheng, R. Photocatalytic membrane reactor (PMR) for virus removal in water: Performance and mechanisms. *Chem. Eng. J.* **2015**, *277*, 124–129. [CrossRef]
114. Jiang, L.; Choo, K.H. Photocatalytic mineralization of secondary effluent organic matter with mitigating fouling propensity in a submerged membrane photoreactor. *Chem. Eng. J.* **2016**, *288*, 798–805. [CrossRef]
115. Molinari, R.; Caruso, A.; Argurio, P.; Poerio, T. Degradation of the drugs Gemfibrozil and Tamoxifen in pressurized and de-pressurized membrane photoreactors using suspended polycrystalline TiO_2 as catalyst. *J. Membr. Sci.* **2008**, *319*, 54–63. [CrossRef]
116. Mozia, S.; Darowna, D.; Orecki, A.; Wróbel, R.; Wilpiszewska, K.; Morawski, A.W. Microscopic studies on TiO_2 fouling of MF/UF polyethersulfone membranes in a photocatalytic membrane reactor. *J. Membr. Sci.* **2014**, *470*, 356–368. [CrossRef]
117. Mahlangu, O.T.; Motsa, M.M.; Nkambule, T.I.; Mamba, B.B. Rejection of trace organic compounds by membrane processes: Mechanisms, challenges, and opportunities. *Rev. Chem. Eng.* **2023**, *39*, 875–910. [CrossRef]
118. Verliefde, A.R.D.; Cornelissen, E.R.; Heijman, S.G.J.; Verberk, J.; Amy, G.L.; Van der Bruggen, B.; Van Dijk, J.C. The role of electrostatic interactions on the rejection of organic solutes in aqueous solutions with nanofiltration. *J. Membr. Sci.* **2008**, *322*, 52–66. [CrossRef]
119. Nguyen, V.-H.; Tran, Q.B.; Nguyen, X.C.; Hai, L.T.; Ho, T.T.T.; Shokouhimehr, M.; Vo, D.-V.N.; Lam, S.S.; Nguyen, H.P.; Hoang, C.T.; et al. Submerged photocatalytic membrane reactor with suspended and immobilized N-doped TiO_2 under visible irradiation for diclofenac removal from wastewater. *Process Saf. Environ. Prot.* **2020**, *142*, 229–237. [CrossRef]
120. Mozia, S.; Rajakumaran, R.; Szymański, K.; Gryta, M. Removal of ketoprofen from surface water in a submerged photocatalytic membrane reactor utilizing membrane distillation: Effect of process parameters and evaluation of long-term performance. *J. Chem. Technol. Biotechnol.* **2023**, *98*, 1125–1136. [CrossRef]
121. Tai, Z.S.; Othman, M.H.D.; Koo, K.N.; Jaafar, J. Critical review on membrane designs for enhanced flux performance in membrane distillation. *Desalination* **2023**, *553*, 116484. [CrossRef]
122. Szymański, K.; Gryta, M.; Darowna, D.; Mozia, S. A new submerged photocatalytic membrane reactor based on membrane distillation for ketoprofen removal from various aqueous matrices. *Chem. Eng. J.* **2022**, *435*, 134872. [CrossRef]

123. Buiteveld, H.; Hakvoort, J.H.M.; Donze, M. Optical properties of pure water. In Proceedings of the Ocean Optics XII, Bergen, Norway, 13–15 June 1994; pp. 174–183.
124. Dijkstra, M.F.J.; Michorius, A.; Buwalda, H.; Panneman, H.J.; Winkelman, J.G.M.; Beenackers, A.A.C.M. Comparison of the efficiency of immobilized and suspended systems in photocatalytic degradation. *Catal. Today* **2001**, *66*, 487–494. [CrossRef]
125. Hofstadler, K.; Bauer, R.; Novalic, S.; Heisler, G. New Reactor Design for Photocatalytic Wastewater Treatment with TiO_2 Immobilized on Fused-Silica Glass Fibers: Photomineralization of 4-Chlorophenol. *Environ. Sci. Technol.* **1994**, *28*, 670–674. [CrossRef]
126. Manassero, A.; Satuf, M.L.; Alfano, O.M. Photocatalytic reactors with suspended and immobilized TiO_2: Comparative efficiency evaluation. *Chem. Eng. J.* **2017**, *326*, 29–36. [CrossRef]
127. Ali, H.M.; Arabpour Roghabadi, F.; Ahmadi, V. Solid-supported photocatalysts for wastewater treatment: Supports contribution in the photocatalysis process. *Sol. Energy* **2023**, *255*, 99–125. [CrossRef]
128. Uheida, A.; Mejía, H.G.; Abdel-Rehim, M.; Hamd, W.; Dutta, J. Visible light photocatalytic degradation of polypropylene microplastics in a continuous water flow system. *J. Hazard. Mater.* **2021**, *406*, 124299. [CrossRef]
129. Shen, M.; Zhang, G.; Liu, J.; Liu, Y.; Zhai, J.; Zhang, H.; Yu, H. Visible-light-driven photodegradation of xanthate in a continuous fixed-bed photoreactor: Experimental study and modeling. *Chem. Eng. J.* **2023**, *461*, 141833. [CrossRef]
130. Ljubas, D.; Juretić, H.; Badrov, A.; Biošić, M.; Babić, S. Photocatalytic Degradation of Pharmaceutical Trimethoprim in Aqueous Solution over Nanostructured TiO_2 Film Irradiated with Simulated Solar Radiation. *Appl. Sci.* **2023**, *13*, 5681. [CrossRef]
131. Easton, T.; Koutsos, V.; Chatzisymeon, E. Removal of polyester fibre microplastics from wastewater using a UV/H_2O_2 oxidation process. *J. Environ. Chem. Eng.* **2023**, *11*, 109057. [CrossRef]
132. García-Muñoz, P.; Allé, P.H.; Bertoloni, C.; Torres, A.; de la Orden, M.U.; Urreaga, J.M.; Dziurla, M.-A.; Fresno, F.; Robert, D.; Keller, N. Photocatalytic degradation of polystyrene nanoplastics in water. A methodological study. *J. Environ. Chem. Eng.* **2022**, *10*, 108195. [CrossRef]
133. Sampaio, M.J.; Ribeiro, A.R.L.; Ribeiro, C.M.R.; Borges, R.A.; Pedrosa, M.F.; Silva, A.M.T.; Silva, C.G.; Faria, J.L. A technological approach using a metal-free immobilized photocatalyst for the removal of pharmaceutical substances from urban wastewaters. *Chem. Eng. J.* **2023**, *459*, 141617. [CrossRef]
134. Silva, F.V.; Lansarin, M.A.; Moro, C.C. A comparison of slurry and immobilized TiO_2 in the photocatalytic degradation. *Lat. Am. Appl. Res.* **2012**, *42*, 275–280.
135. Miranda-García, N.; Maldonado, M.I.; Coronado, J.M.; Malato, S. Degradation study of 15 emerging contaminants at low concentration by immobilized TiO_2 in a pilot plant. *Catal. Today* **2010**, *151*, 107–113. [CrossRef]
136. Cho, I.-H.; Park, J.-H.; Kim, Y.-G. Oxidative degradation and toxicity reduction of trichloroethylene (TCE) in water using TiO_2/solar light: Comparative study of TiO_2 slurry and immobilized systems. *J. Environ. Sci. Health Part A* **2005**, *40*, 1033–1044. [CrossRef]
137. Tasso Guaraldo, T.; Wenk, J.; Mattia, D. Photocatalytic ZnO Foams for micropollutant degradation. *Adv. Sustain. Syst.* **2021**, *5*, 2000208. [CrossRef]
138. Arabatzis, I.M.; Antonaraki, S.; Stergiopoulos, T.; Hiskia, A.; Papaconstantinou, E.; Bernard, M.C.; Falaras, P. Preparation, characterization and photocatalytic activity of nanocrystalline thin film TiO_2 catalysts towards 3,5-dichlorophenol degradation. *J. Photochem. Photobiol. A Chem.* **2002**, *149*, 237–245. [CrossRef]
139. Wang, X.H.; Li, J.G.; Kamiyama, H.; Moriyoshi, Y.; Ishigaki, T. Wavelength-Sensitive Photocatalytic Degradation of Methyl Orange in Aqueous Suspension over Iron(III)-doped TiO_2 Nanopowders under UV and Visible Light Irradiation. *J. Phys. Chem. B* **2006**, *110*, 6804–6809. [CrossRef]
140. Fox, M.A.; Dulay, M.T. Heterogeneous photocatalysis. *Chem. Rev.* **1993**, *93*, 341–357. [CrossRef]
141. Bhatkhande, D.S.; Pangarkar, V.G.; Beenackers, A.A.C.M. Photocatalytic degradation for environmental applications—A review. *J. Chem. Technol. Biotechnol. Int. Res. Process Environ. Clean Technol.* **2002**, *77*, 102–116. [CrossRef]
142. Jo, W.-K.; Tayade, R.J. New Generation Energy-Efficient Light Source for Photocatalysis: LEDs for Environmental Applications. *Ind. Eng. Chem. Res.* **2014**, *53*, 2073–2084. [CrossRef]
143. Bilal, M.; Rasheed, T.; Iqbal, H.M.N.; Li, C.; Wang, H.; Hu, H.; Wang, W.; Zhang, X. Photocatalytic degradation, toxicological assessment and degradation pathway of C.I. Reactive Blue 19 dye. *Chem. Eng. Res. Des.* **2018**, *129*, 384–390. [CrossRef]
144. Mioduska, J.; Łapiński, M.S.; Karczewski, J.; Hupka, J.; Zielińska-Jurek, A. New LED photoreactor with modulated UV–vis light source for efficient degradation of toluene over WO3/TiO_2 photocatalyst. *Chem. Eng. Res. Des.* **2023**, *193*, 145–157. [CrossRef]
145. Tapia-Tlatelpa, T.; Buscio, V.; Trull, J.; Sala, V. Performance analysis and methodology for replacing conventional lamps by optimized LED arrays for photocatalytic processes. *Chem. Eng. Res. Des.* **2020**, *156*, 456–468. [CrossRef]
146. Asahi, R.; Morikawa, T.; Ohwaki, T.; Aoki, K.; Taga, Y. Visible-light photocatalysis in nitrogen-doped titanium oxides. *Science* **2001**, *293*, 269–271. [CrossRef]
147. Li, Y.; Sun, S.; Ma, M.; Ouyang, Y.; Yan, W. Kinetic study and model of the photocatalytic degradation of rhodamine B (RhB) by a TiO_2-coated activated carbon catalyst: Effects of initial RhB content, light intensity and TiO_2 content in the catalyst. *Chem. Eng. J.* **2008**, *142*, 147–155. [CrossRef]
148. Liang, R.; Van Leuwen, J.C.; Bragg, L.M.; Arlos, M.J.; Li Chun Fong, L.C.M.; Schneider, O.M.; Jaciw-Zurakowsky, I.; Fattahi, A.; Rathod, S.; Peng, P.; et al. Utilizing UV-LED pulse width modulation on TiO_2 advanced oxidation processes to enhance the decomposition efficiency of pharmaceutical micropollutants. *Chem. Eng. J.* **2019**, *361*, 439–449. [CrossRef]

149. Sannino, D.; Morante, N.; Sacco, O.; Mancuso, A.; De Guglielmo, L.; Di Capua, G.; Femia, N.; Vaiano, V. Visible light-driven degradation of Acid Orange 7 by light modulation techniques. *Photochem. Photobiol. Sci.* **2023**, *22*, 185–193. [CrossRef] [PubMed]
150. Pronk, W.; Ding, A.; Morgenroth, E.; Derlon, N.; Desmond, P.; Burkhardt, M.; Wu, B.; Fane, A.G. Gravity-driven membrane filtration for water and wastewater treatment: A review. *Water Res.* **2019**, *149*, 553–565. [CrossRef] [PubMed]
151. Stoffel, D.; Derlon, N.; Traber, J.; Staaks, C.; Heijnen, M.; Morgenroth, E.; Jacquin, C. Gravity-driven membrane filtration with compact second-life modules daily backwashed: An alternative to conventional ultrafiltration for centralized facilities. *Water Res. X* **2023**, *18*, 100178. [CrossRef] [PubMed]
152. Toray Membrane USA. Treated Municipal Sewage Achieves High-Quality Discharge Values with Toray MBR Technology. Available online: https://vertassets.blob.core.windows.net/download/b1be1370/b1be1370-c513-46d4-93f3-653377273b5a/mirassol__brazil___toray_mbr.pdf (accessed on 14 July 2023).
153. Al-Obaidi, M.A.; Alsarayreh, A.A.; Al-Hroub, A.M.; Alsadaie, S.; Mujtaba, I.M. Performance analysis of a medium-sized industrial reverse osmosis brackish water desalination plant. *Desalination* **2018**, *443*, 272–284. [CrossRef]
154. Al-Obaidi, M.A.; Kara-Zaïtri, C.; Mujtaba, I.M. Wastewater treatment by spiral wound reverse osmosis: Development and validation of a two dimensional process model. *J. Clean. Prod.* **2017**, *140*, 1429–1443. [CrossRef]
155. Lin, W.; Zhang, Y.; Li, D.; Wang, X.-m.; Huang, X. Roles and performance enhancement of feed spacer in spiral wound membrane modules for water treatment: A 20-year review on research evolvement. *Water Res.* **2021**, *198*, 117146. [CrossRef]
156. Li, W.; Zhao, W.; Zhu, H.; Li, Z.-J.; Wang, W. State of the art in the photochemical degradation of (micro)plastics: From fundamental principles to catalysts and applications. *J. Mater. Chem. A* **2023**, *11*, 2503–2527. [CrossRef]
157. Legrini, O.; Oliveros, E.; Braun, A.M. Photochemical processes for water treatment. *Chem. Rev.* **1993**, *93*, 671–698. [CrossRef]
158. Cao, R.; Zhang, M.-Q.; Hu, C.; Xiao, D.; Wang, M.; Ma, D. Catalytic oxidation of polystyrene to aromatic oxygenates over a graphitic carbon nitride catalyst. *Nat. Commun.* **2022**, *13*, 4809. [CrossRef]
159. Habibi, M.; Habibi-Yangjeh, A.; Khataee, A. S-scheme CeO_2-x/$AgFeO_2$/Ag photocatalysts with impressive activity in degradation of different antibiotics under visible light. *Surf. Interfaces* **2023**, *39*, 102937. [CrossRef]
160. Baaloudj, O.; Kenfoud, H.; Badawi, A.K.; Assadi, A.A.; El Jery, A.; Assadi, A.A.; Amrane, A. Bismuth Sillenite Crystals as Recent Photocatalysts for Water Treatment and Energy Generation: A Critical Review. *Catalysts* **2022**, *12*, 500. [CrossRef]
161. Mestre, A.S.; Carvalho, A.P. Photocatalytic Degradation of Pharmaceuticals Carbamazepine, Diclofenac, and Sulfamethoxazole by Semiconductor and Carbon Materials: A Review. *Molecules* **2019**, *24*, 3702. [CrossRef] [PubMed]
162. Baek, S.; Ghaffari, Y.; Kim, E.; Kim, K.; Bae, J. Photocatalytic Adsorbent for the Removal of Micro-Pollution from Industrial WWTPs. In Proceedings of the 8th World Congress on Civil, Structural, and Environmental Engineering (CSEE'23), Lisbon, Portugal, 29–31 March 2023.
163. Qanbarzadeh, M.; DiGiacomo, L.; Bouteh, E.; Alhamdan, E.Z.; Mason, M.M.; Wang, B.; Wong, M.S.; Cates, E.L. An Ultraviolet/Boron Nitride Photocatalytic Process Efficiently Degrades Poly-/Perfluoroalkyl Substances in Complex Water Matrices. *Environ. Sci. Technol. Lett.* **2023**, *10*, 705–710. [CrossRef]
164. He, J.; Han, L.; Wang, F.; Ma, C.; Cai, Y.; Ma, W.; Xu, E.G.; Xing, B.; Yang, Z. Photocatalytic strategy to mitigate microplastic pollution in aquatic environments: Promising catalysts, efficiencies, mechanisms, and ecological risks. *Crit. Rev. Environ. Sci. Technol.* **2023**, *53*, 504–526. [CrossRef]
165. Packialakshmi, J.S.; Albeshr, M.F.; Alrefaei, A.F.; Zhang, F.; Liu, X.; Selvankumar, T.; Mythili, R. Development of ZnO/SnO_2/rGO hybrid nanocomposites for effective photocatalytic degradation of toxic dye pollutants from aquatic ecosystems. *Environ. Res.* **2023**, *225*, 115602. [CrossRef]
166. Gordanshekan, A.; Arabian, S.; Nazar, A.R.S.; Farhadian, M.; Tangestaninejad, S. A comprehensive comparison of green Bi2WO6/g-C3N4 and Bi2WO6/TiO_2 S-scheme heterojunctions for photocatalytic adsorption/degradation of Cefixime: Artificial neural network, degradation pathway, and toxicity estimation. *Chem. Eng. J.* **2023**, *451*, 139067. [CrossRef]
167. Leelavathi, H.; Muralidharan, R.; Abirami, N.; Tamizharasan, S.; Sankeetha, S.; Kumarasamy, A.; Arulmozhi, R. Construction of step-scheme g-C3N4/Co/ZnO heterojunction photocatalyst for aerobic photocatalytic degradation of synthetic wastewater. *Colloids Surf. A Physicochem. Eng. Asp.* **2023**, *656*, 130449. [CrossRef]
168. Maulana, D.A.; Ibadurrohman, M. Synthesis of nano-composite Ag/TiO_2 for polyethylene microplastic degradation applications. *IOP Conf. Ser. Mater. Sci. Eng.* **2021**, *1011*, 012054. [CrossRef]
169. Vital-Grappin, A.D.; Ariza-Tarazona, M.C.; Sandoval, I.; Rojas-Guerrero, C.A.; Villarreal-Chiu, J.F.; Cedillo-González, E.I. Design of Green TiO_2-Based Semiconductors for Microplastic and Nanoplastic Photocatalytic Degradation. *Preprints* **2023**, 2023010544. [CrossRef]
170. Despotović, V.; Finčur, N.; Bognar, S.; Šojić Merkulov, D.; Putnik, P.; Abramović, B.; Panić, S. Characterization and Photocatalytic Performance of Newly Synthesized ZnO Nanoparticles for Environmental Organic Pollutants Removal from Water System. *Separations* **2023**, *10*, 258. [CrossRef]
171. Guo, Y.; Wen, M.; Li, G.; An, T. Recent advances in VOC elimination by catalytic oxidation technology onto various nanoparticles catalysts: A critical review. *Appl. Catal. B Environ.* **2021**, *281*, 119447. [CrossRef]
172. Carp, O.; Huisman, C.L.; Reller, A. Photoinduced reactivity of titanium dioxide. *Prog. Solid State Chem.* **2004**, *32*, 33–177. [CrossRef]
173. Ren, L.; Huo, W.; Li, G.; Choi, W.; An, T. Photocatalytic mechanisms and photocatalyst deactivation during the degradation of 5-fluorouracil in water. *Catal. Today* **2023**, *410*, 45–55. [CrossRef]

174. Katz, A.; McDonagh, A.; Tijing, L.; Shon, H.K. Fouling and inactivation of titanium dioxide-based photocatalytic systems. *Crit. Rev. Environ. Sci. Technol.* **2015**, *45*, 1880–1915. [CrossRef]
175. Liqiang, J.; Baifu, X.; Fulong, Y.; Baiqi, W.; Keying, S.; Weimin, C.; Honggang, F. Deactivation and regeneration of ZnO and TiO_2 nanoparticles in the gas phase photocatalytic oxidation of n-C7H16 or SO_2. *Appl. Catal. A Gen.* **2004**, *275*, 49–54. [CrossRef]
176. Yan, X.; Tang, Y.; Ma, C.; Liu, Y.; Xu, J. Deactivation and regeneration of photocatalysts: A review. *Desalination Water Treat.* **2018**, *124*, 160–176. [CrossRef]
177. Yan, X.; Li, J.; Ma, C.; Tang, Y.; Kong, X.; Lu, J. Study on the lifetime of photocatalyst by photocatalytic membrane reactors (PMR). *Water Sci. Technol.* **2020**, *81*, 131–137. [CrossRef]
178. Miranda-García, N.; Suárez, S.; Maldonado, M.I.; Malato, S.; Sánchez, B. Regeneration approaches for TiO_2 immobilized photocatalyst used in the elimination of emerging contaminants in water. *Catal. Today* **2014**, *230*, 27–34. [CrossRef]
179. Liang, C.; Li, C.; Zhu, Y.; Du, X.; Yao, C.; Ma, Y.; Zhao, J. Recent advances of photocatalytic degradation for BTEX: Materials, operation, and mechanism. *Chem. Eng. J.* **2023**, *455*, 140461. [CrossRef]
180. Kanna, M.; Wongnawa, S.; Buddee, S.; Dilokkhunakul, K.; Pinpithak, P. Amorphous titanium dioxide: A recyclable dye remover for water treatment. *J. Sol-Gel Sci. Technol.* **2010**, *53*, 162–170. [CrossRef]
181. Prieto, O.; Fermoso, J.; Irusta, R. Photocatalytic Degradation of Toluene in Air Using a Fluidized Bed Photoreactor. *Int. J. Photoenergy* **2007**, *2007*, 032859. [CrossRef]
182. Rueda-Marquez, J.J.; Levchuk, I.; Fernández Ibañez, P.; Sillanpää, M. A critical review on application of photocatalysis for toxicity reduction of real wastewaters. *J. Clean. Prod.* **2020**, *258*, 120694. [CrossRef]
183. Plakas, K.V.; Georgiadis, A.A.; Karabelas, A.J. Sustainability assessment of tertiary wastewater treatment technologies: A multi-criteria analysis. *Water Sci. Technol.* **2016**, *73*, 1532–1540. [CrossRef] [PubMed]
184. Karabelas, A.J.; Plakas, K.V.; Sarasidis, V.C. How far are we from large-scale PMR applications? In *Current Trends and Future Developments on (Bio-) Membranes*; Elsevier: Amsterdam, The Netherlands, 2018; pp. 233–295.
185. Samhaber, W.M.; Nguyen, M.T. Economical Aspects in Photocatalytic Membrane Reactors. In *Current Trends and Future Developments on (Bio-) Membranes: Photocatalytic Membranes and Photocatalytic Membrane Reactors*; Elsevier: Amsterdam, The Netherlands, 2018; pp. 317–345.
186. Rani, C.N.; Karthikeyan, S. Synergic effects on degradation of a mixture of polycyclic aromatic hydrocarbons in a UV slurry photocatalytic membrane reactor and its cost estimation. *Chem. Eng. Process.-Process Intensif.* **2020**, *159*, 108179. [CrossRef]